LIGO-T960215-A-D

HYTEC-TN-LIGO-07a
09/13/96
Revision *a*, 01/15/97

BSC Seismic Isolation Projected Performance Update

Eric Ponslet
September 13, 1996
Revision *a*, January 15, 1997

Abstract

This notes summarizes performance predictions of the current designs for the BSC seismic isolation systems. Three configurations using the baseline Viton rubber spring and two damped metal spring designs (multi-layer coil spring and leaf spring) are considered. Vertical and horizontal transmissibilities are evaluated as well as residual test mass motion due to floor seismic noise in horizontal and vertical directions. The effects of stack imperfections (variability in springs, misalignments, etc.) are also considered. Transmissibilities are given for the isolation stack alone (SIS) as well as for the complete isolation system (SEI), including a rough dynamic model of the support structure and actuator systems.

HYTEC Inc.
110 Eastgate Dr., Ste 100
Los Alamos, NM 87544
(505) 662-0080 / Fax (505) 662-5179

LIGO PROJECT

1. BSC Seismic Isolation - System Description

The current design layout for the BSC SEI is shown in Fig. 1. The global coordinate system used throughout this document is shown in the figure. Its origin is on the facility floor along the vertical axis of the downtube, the *Z* axis is pointing vertically up and the *X* axis is parallel to the internal support beams. Rotations *a* (roll), *b* (pitch), and *c* (yaw) are also defined.

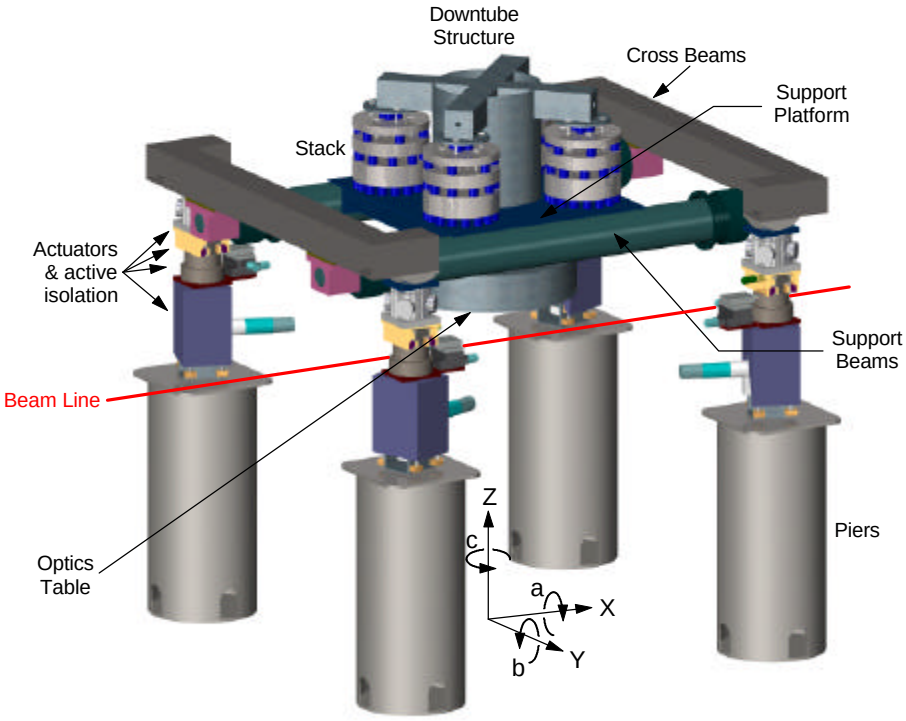

Figure 1: overall configuration of BSC seismic isolation system.

We distinguish two separate subsystems: the support structure and the isolation stack. The support structure consists of the piers, coarse and fine actuation systems, active isolation, external cross beams, internal support beams, and support platform. It is described in reference 1. The stack[2] consists of 4 legs of springs and stainless steel masses, the downtube/optics table structure, and the payload (optics, etc.). The stack and downtube structure[3] as well as the cross beams, support beams and support platform have all been designed in some detail and analyzed with finite element models. Their mass properties and first resonant frequencies are listed in Table 1.

The actuator systems are at a less mature stage of design and complete dynamic models have not been developed. Their representation in the simulation models is based on very rough assumptions and approximations.

subsystem	Total Mass	Moments of Inertia @ CG	First Resonance
	kg	$kg.m^2$	Hz
downtube & optics table with 500 lb payload	651.	$I_{XX} = I_{YY} = 188.8$ $I_{ZZ} = 129.4$	349
support structure (cross beams, support beams, support platform)	2135.	-	15

Table 1: Mass properties and resonant frequencies of the support structure and downtube/optics table.

The stack provides seismic isolation for the optics table and is responsible for the largest part of this isolation at low frequencies. However, the support structure is not infinitely rigid and contributes to isolation at higher frequencies (above 50 Hz or so) while its resonances degrade isolation at lower frequencies[1]. The major sources of compliance in the support system are the piers, actuator system, and active isolation units (horizontal compliance) and the cross beams and support tubes (vertical compliance)[1].

2. Design Requirements

The basic design requirement is a limit on the RMS spectrum of the residual *X* motion of the test mass[4] shown in Fig. 2.

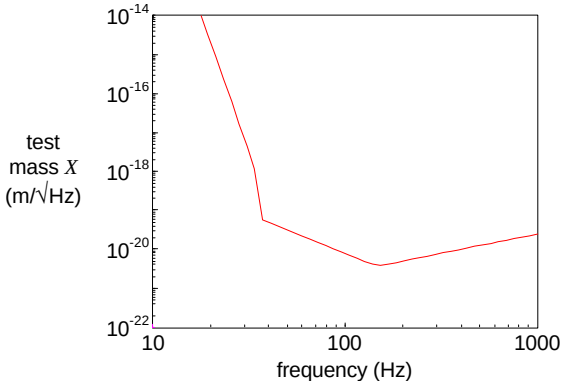

Figure 2: Seismic allowance for test mass displacement[4].

This spectrum can be evaluated by combining the transmissibilities of the SEI (support + stack) with the transfer functions of the SUS and the assumed PSD's of the facility floor X and Z motions defined in the DRD document[4]. From this basic displacement noise limit, requirements have been defined for the horizontal and vertical transmissibilities of the SEI system (Fig. 3 and [4]).

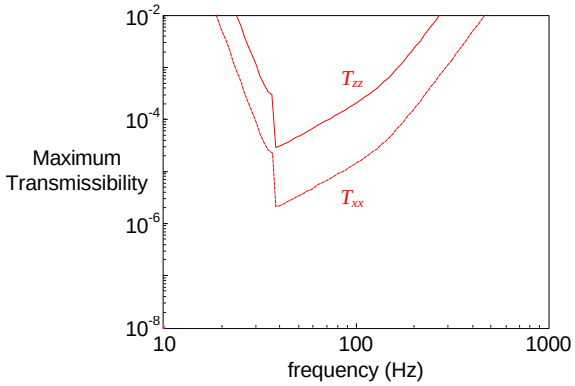

Figure 3: Approximate transmissibility requirements for BSC SEI derived from seismic allowance[4].

Note however that the derivation of those transmissibility requirements was based on relatively crude assumptions on SUS transmissibilities and did not account for vertical-horizontal or horizontal-pitch coupling. Because of this, transmissibility predictions should only be used as rough indicators of the adequacy of a design; final judgment should be based on predicted residual seismic motion of the test mass in the beam (*X*) direction (see Section 3.4).

3. Modeling

3.1 Assumptions

All stack elements and the downtube structure are modeled as rigid bodies[5] (their natural frequencies are above 300 Hz). The support structure dynamics is roughly approximated using a set of two rigid bodies and 8 three-dimensional springs (see Section 3.2). Spring resonances are neglected (springs are designed so that first resonant frequency is above 400 Hz[6]).

The attachment point of the test mass suspension wires is assumed[7] to be at X = 0 cm, Y = 20 cm, and Z = -15 cm with respect to the center of the bottom surface of the optics table. The transmissibilities of the SEI system are evaluated from the facility floor to that point.

3.2 Support Structure Dynamics

The support structure consists of the 4 piers, coarse and fine actuation systems, active isolation units, external cross beams, internal support beams, and support platform[1] (see Fig. 1). Because of its large size, this support cannot be made “infinitely” stiff (i.e. first natural frequency well above stack resonances) and its resonances affect the overall isolation performance. To estimate the impact of these support resonances on SEI performance, a 12 degree of freedom (d.o.f.) approximation of the support system dynamics was included in the 3D Matlab models of the SEI (Fig. 4).

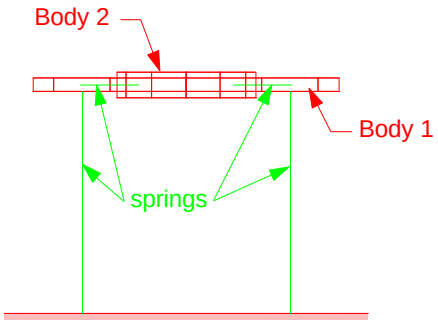

Figure 4: 12 d.o.f. approximate dynamic model of BSC support structure

The support system is arbitrarily divided into two 6 d.o.f. rigid bodies, connected together and to the facility floor with 2 sets of 4, 3-dimensional springs with structural damping. The first body (#1 in Fig. 4) loosely corresponds to the piers, actuators and cross-beams while the second represents the support beams and platform.

The spring constants in 3 directions for each set of four springs are extracted from static deflection results obtained from COSMOS FEM models. Initial mass properties for the two bodies are roughly calculated based on the mode shapes predicted by the FEM models, then fine tuned to match FEM predictions of the first few natural frequencies of the complete support system (floor to support platform). With those parameters, the *approximate* dynamic model of the support predicts the natural frequencies listed in Table 2. COSMOS predictions are also included in the table. Note the good agreement on 6 of the 7 lowest modes.

Mode #	Nat. Frequency [Hz]		Mode Shape: major contribution to deformation / motion of support platform
	MATLAB Model	COSMOS Model.	
1	15	15	actuator deformations / shear along Y
2	19	19	actuator deformations / twist around Z
3	24	22	actuator deformations / shear along X
4	not observed	39	twist in cross beams / up & down motion
5	41	41	twist in cross beams / rocking around Y
6	66	65	bending in support beams / up & down motion
7	69	68	bending in support beams / rocking around X

Table 2: Assumed imperfections in isolation stacks.

3.3 Modeling of Stack and Support Imperfections

Imperfections must be accounted for in the simulations because they create asymmetries that result in various coupling transmissibilities which do not appear in a perfect, symmetric stack. Imperfections in the masses and alignment of all SEI components, spring stiffnesses and loss factors, and spring verticality and alignment are accounted for in this analysis. Monte Carlo simulations are used to evaluate Min-Max ranges for the various transmissibility terms and for the residual motion of the test mass in the beam (*X*) direction.

Each imperfect parameter is given a random value p in a uniform distribution, centered around the nominal values p_o and with deviation Δp, i.e.

$$p = p_o + \text{uniform}[-\Delta p....+\Delta p], \qquad (1)$$

where uniform[-Δp…+Δp] is a uniformly distributed random number between -Δp and Δp. The imperfections assumed in the model are listed in Table 3 for the stack and Table 4 for the support system. For each parameter, the tables give the nominal value p_o and the assumed deviation Δp (or relative deviation $\Delta p/p_o$). Note that all values are nothing more than engineering estimates and that, for a fair comparison, the same relative deviations on stiffness, damping, and verticality have been assumed for all 3 types of springs.

Parameter	Nominal value p_o	Deviation Δp or $\Delta p/p_o$ (%)
leg element *X* and *Y* position, stage 1	X_{leg} , Y_{leg}	1 mm
" " " " stage 2	"	2 mm
" " " " stage 3	"	3 mm
spring *X* and *Y* position, stage 1	uniform on circle	2 mm
" " " stage 2	"	3 mm
" " " stage 3	"	4 mm
" " " stage 4	"	5 mm
downtube *X* and *Y* position	$X = Y = 0$	5 mm
leg element mass	see tables 2, 3, and 4	0.1 %
downtube mass (incl. payload)	605.6 kg	1 %
spring stiffnesses K_x, K_y, K_z	table lookup VS freq.	3 %
spring loss factors h_x, h_y, h_z	table lookup VS freq.	5 %
spring verticality	vertical	2º
spring orientation (leaf springs only)	radial	5º

Table 3: Assumed imperfections in isolation stacks.

Parameter	Nominal value	Deviation
	p_o	Δp or $\Delta p/p_o$ (%)
X and Y position, body 1	$X = Y = 0$	5 mm*
" " " body 2	$X = Y = 0$	10 mm*
mass, body 1	1984. kg	1 %
mass, body 2	433. kg	1 %
spring stiffnesses, floor to body 1	K_x=14, K_y=5, K_z=990 N/µm	3 %
spring loss factors, floor to body 1	0.050	5 %
spring verticality, floor to body 1	vertical	0.1º
spring stiffnesses, body 1 to body 2	K_x=62, K_y=42, K_z=19 N/µm	3 %
spring loss factors, body 1 to body 2	0.005	5 %
max. coupling terms, body 1 to body 2	no coupling	0.5 % of K_z

* accounts for actuation range in addition to tolerances

Table 4: Assumed imperfections in support system.

3.4 Evaluation of Residual Test Mass Motion

The SUS pendulum is attached to the optics table of the SIS. Assuming that the moving masses in the SUS are small in magnitude compared to the downtube, we can treat the complete assembly as 2 linear systems connected in series. Calculation of the spectrum of X motion of the test mass then requires a series of transfer functions for both subsystems. The following assumptions are made:

- the only important contributions from the floor seismic motion are the X and Z motions. The X and Z noise spectra are assumed identical[4].
- the SUS transfer functions produce horizontal test mass motion from optics plate motion in the horizontal (T_{xx}^{SUS}), vertical (T_{xz}^{SUS}), yaw (T_{xc}^{SUS}), and pitch (T_{xb}^{SUS}) directions. The magnitudes of these transfer functions[8,10] are plotted in Fig. 5. Note that T_{xx}^{SUS} is at least 1 order of magnitude larger than the other transfer functions.
- the horizontal and vertical motions of the floor are assumed uncorrelated.

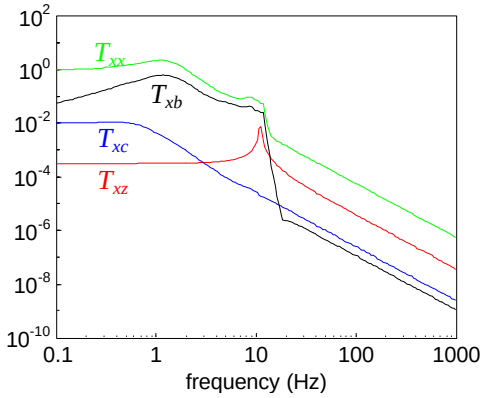

Figure 5: transmissibilities of the SUS system (X motion of test mass in response to optics table motion in X, Z, b (pitch), and c (yaw) directions[8,10]).

With these assumptions, the PSD of the residual test mass motion in the horizontal (*X*) direction (X^2_{mass}) is evaluated from the PSDs of floor motion in the horizontal and vertical directions (X^2_{floor} and Z^2_{floor}) as

$$X^2_{mass} = \left[T^{SEI+SUS}\right] \cdot \begin{bmatrix} X^2_{floor} & 0 \\ 0 & Z^2_{floor} \end{bmatrix} \cdot \left[T^{SEI+SUS}\right]^*, \qquad (1)$$

where * denotes the adjoint operator and $\left[T^{SEI+SUS}\right]$ is a matrix of transfer functions for the complete isolation and suspension system and is evaluated as

$$\left[T^{SEI+SUS}\right] = \left[T^{SUS}_{xx} \quad T^{SUS}_{xz} \quad T^{SUS}_{xb} \quad T^{SUS}_{xc}\right] \cdot \begin{bmatrix} T^{SEI}_{xx} & T^{SEI}_{xz} \\ T^{SEI}_{zx} & T^{SEI}_{zz} \\ T^{SEI}_{bx} & T^{SEI}_{bz} \\ T^{SEI}_{cx} & T^{SEI}_{cz} \end{bmatrix}, \qquad (2)$$

where all *T* 's are complex functions of frequency. The complete 4×2 matrix of SEI transfer functions is evaluated with our 3D Matlab code. The RMS spectrum of test mass motion in the *X* direction can be compared directly to the requirement of Fig. 2.

3.5 Calculation of Figures of Merit for Lock Acquisition

The lock acquisition figure of merit is the RMS velocity of the test mass in response to residual seismic noise, with the test mass pendulum damped by the SUS control system. This RMS velocity is in principle derived directly from the test mass motion PSD, X^2_{mass}, as

$$V_{RMS} = \sqrt{\int_{f=0}^{\infty} 4\pi f^2 X^2_{mass}\, df}\ . \qquad (3)$$

In practice, we use a simple trapezoidal rule to perform numerical integration from 0 to 10 Hz. The frequency axis is densely sampled to insure sufficient density of data to pick up the micro-seismic peak and stack resonances. Based on previous experience, it is believed[4] that RMS velocities of the order of 1 μm/sec should guarantee reasonable lock acquisition performance.

3.6 Calculation of Figures of Merit for Lock Maintenance

Whether the SUS actuators can maintain a lock condition depends on the amount of force required to control the test mass and the force capacity of these actuators. A figure of merit χ_{RMS} is defined as the RMS value of a weighted test mass displacement measure $\chi(s)$ calculated as

$$\chi(s) = F^{-1}(s)\left(T^{SUS}_{xx}(s)\right)^{-1}\sqrt{X^2_{mass}(s)}\,, \qquad (4)$$

where $F^{-1}(s)$ is the inverse of the SUS actuation compensation. The RMS value of $\chi(s)$ is computed by integration as

$$\chi_{RMS} = \sqrt{\int_{f=0}^{\infty} \chi(s)^2\, df}\ . \qquad (5)$$

The SEI design requirement document[4] imposes an upper limit of 2.666 μm on χ_{RMS}.

As for the lock acquisition requirement, integral (5) is evaluated numerically using a trapezoidal rule. For typical stacks, χ_{RMS} is dominated by the micro-seismic peak with small contributions from the first stack resonances. This implies that χ_{RMS} is only weakly influenced by stack design (like the Q's of the low frequency stack resonances).

4. Viton Spring Stack

4.1 Properties of Viton Springs

Description of these springs and calculation of their stiffnesses and loss factors are given in [6].

4.2 Stack Design

The design procedure outlined in [5] with a maximum load per spring equal to 556 N (125 lbs) leads to the stack design of Table 5. The total mass of 2909 kg (6413 lbs, includes stack, downtube, and payload) is adopted as an upper limit for the other two stacks in this document.

i (stage #)	M_i, kg (lb) (per leg)	# *springs / leg*	f_i (Hz)	P_i/P_{max} (%)
4 (top)	163 (359)	3	17.0	96
3	108 (239)	5	25.9	96
2	174 (383)	8	25.9	98
1 (base)	282 (622)	13	25.9	99

Number of legs:	4
Total mass:	2909 kg
Total # springs:	116
$\log_{10}(T_{zz})$ @ 35Hz:	-1.44

Table 5: BSC stack design with VITON springs.

The table lists for each stage the mass per leg of the leg elements (or ¼ of the downtube weight for stage 4), the number of springs per leg, the uncoupled stage natural frequency f_i, and the load per spring expressed as a percentage of the assumed ultimate static load capacity.

In order to guarantee back and forth compatibility between the Viton and coil spring stacks (so as to maintain the Viton stack as a candidate last-minute fall-back position), and because the loaded Viton springs are substantially shorter than the loaded coil springs, we propose a Viton stack where the upper stage of 3 springs per leg is replaced with a two-layer stage of 3 springs on top of 3 more (see Fig. 6). The two layers are separated by a small circular plate. The mass of this plate is small enough that it does not behave as an additional stack stage (i.e. it does not introduce new dynamics at low frequency). The result is a top stage that behaves like it was made with springs 2 times softer than the original Viton spring, and a slight improvement in isolation performance.

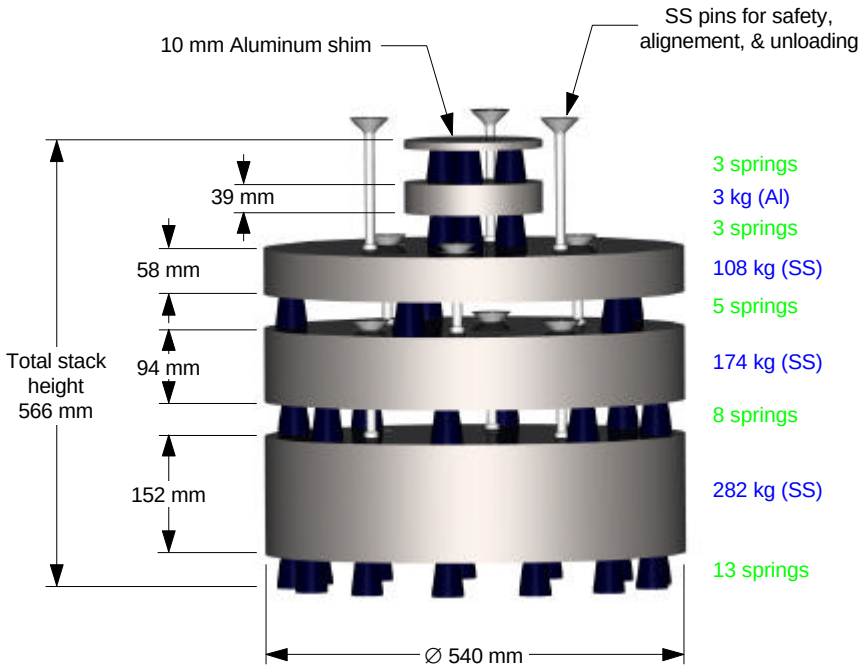

Figure 6: One leg of a VITON spring stack with double top stage.

The natural frequency of the longest safety pins (cantilevered) have been evaluated to about 180 Hz. Because at that frequency the actual horizontal isolation performance of the stacks is about 4 orders of magnitude better than required, and because the pins only represent a small portion of the total stack mass, those resonances are not expected to create violations of the design requirements.

4.3 Performance Predictions

Nominal isolation performance in the horizontal and vertical directions is shown in Fig. 7. Transmissibilities are shown both with and without support flexibility included in the model. When support flexibility is included, additional resonant peaks are observed in the curves: in particular, a prominent peak at about 15 Hz in T_{xx} significantly degrades performance; it is mostly due to horizontal flexibility of the coarse actuator stages[1]. At higher frequencies (typically above 100 Hz) however, the flexible support acts as additional isolation stages, increasing the roll-off rate and improving performance.

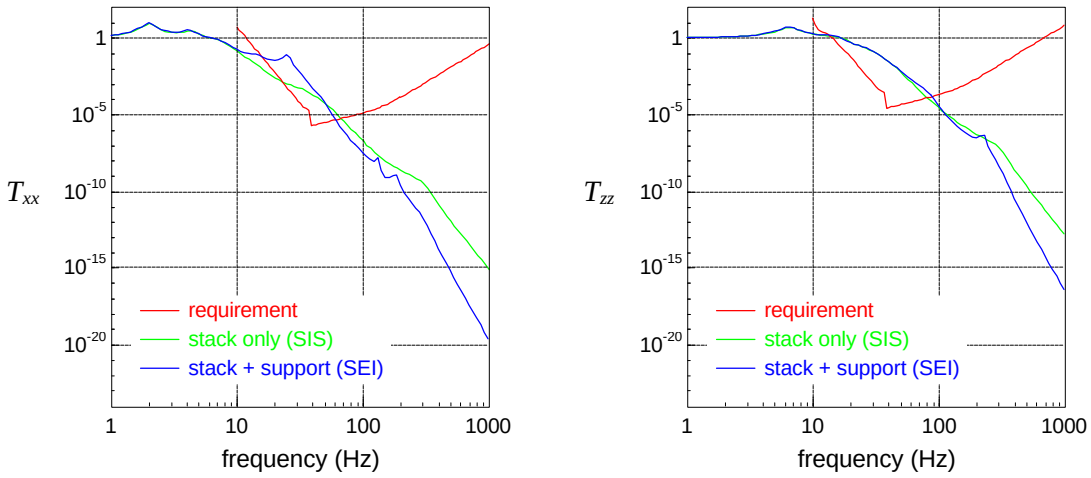

Figure 7: Nominal isolation performance of BSC stack with VITON springs compared to requirements.

Complete simulation results for imperfect stacks are given in Appendix A.1 for a stiff support structure and A.2 for a flexible support (also see Section 8 for an important note). As expected, the introduction of imperfections in the stacks generates new coupling terms (T_{zx} , T_{cx} , T_{xz} , T_{bz} , T_{cz} , T_{zb} , and T_{cb}) which vanish in a perfect stack. The noisy black curves in the figures corresponding to those terms (Appendices A.1 and A.2) are due to numerical noise. Also note that the other terms (T_{xx} , T_{bx} , T_{zz} , T_{xb} , and T_{bb}) are fairly insensitive to imperfections.

Figure 8 shows the estimated residual mass motion due to seismic noise (with flexible support, green curve). The Viton stack violates the requirements by about 3.5 orders of magnitude around 35 Hz. The figure also shows the contributions from floor X noise (black curve) and floor Z noise (blue curve); we can see that below about 10 Hz, the dominant contribution is direct transmission of horizontal seismic noise through the SEI & SUS systems, while above 10 Hz conversion of vertical seismic noise into horizontal test mass motion dominates.

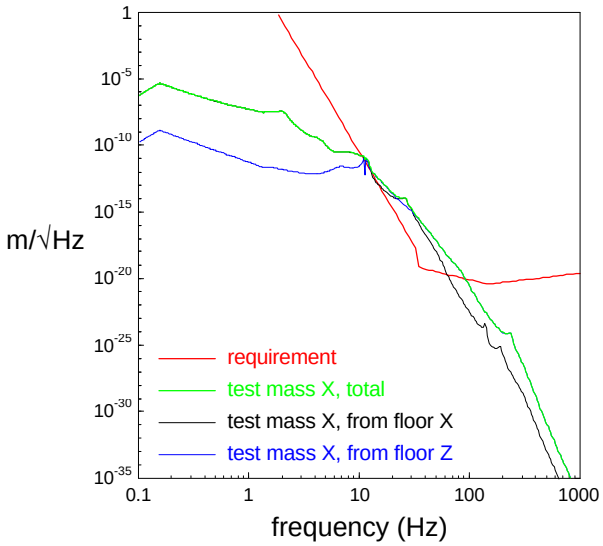

Figure 8: Spectrum of residual test mass X motion for VITON spring stack with flexible support; the green curve shows total residual seismic noise while the black and blue curves show contributions from horizontal and vertical floor noise, respectively.

The PSD of test mass motion is then integrated (using very fine frequency resolution, however result is approximate) to evaluate the lock acquisition and maintenance criteria[4]. The values obtained are listed in Table 6 and compared to requirements.

	value	requirement
Lock Acquisition	1.25 μm/sec	~ 1 μm/sec
Lock Maintenance	2.12 μm	< 2.7 μm

Table 6: BSC stack with VITON springs. Lock acquisition and maintenance requirements (no difference between stack only and support included).

Note that the lock acquisition and maintenance figures of merit for this Viton stack are almost completely dominated by the micro-seismic peak. The first stack resonance occurs at 2.0 Hz with a Q of less than 13 and does not contribute a large portion of those RMS values.

5. Coil Spring Stack

5.1 Properties of Coil Spring

The coil spring is described in detail in [6]. Its geometry is shown in Fig. 9. The expected static axial load capacity is 445 N (100 lbs).

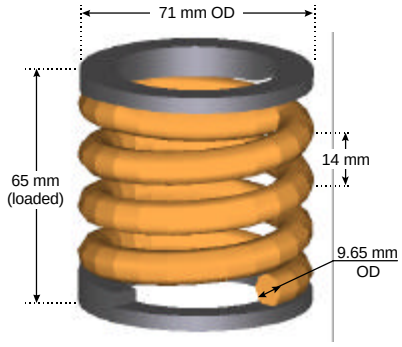

Figure 9: coil spring design.

Stiffnesses and loss factors in the axial direction are evaluated analytically as described in [6]. Ratios of shear to axial stiffnesses and loss factors were obtained from a series of single stage platform tests[9]. Those ratios are assumed frequency independent and set to $k_{shear}/k_{axial} = 2.1$ and $\eta_{shear}/\eta_{axial} = 0.7$.

5.2 Stack Design

The design procedure outlined in [5] with a maximum load per spring equal to 445 N (100 lbs) leads to the stack design of Table 7. Note that the total weight of this stack is identical to that of the baseline Viton stack of Table 5.

i (stage #)	M_i, kg (lb) (per leg)	# *springs / leg*	f_i (Hz)	P_i/P_{max} (%)
4 (top)	163 (359)	4	6.7	89
3	108 (239)	6	9.8	98
2	174 (383)	10	9.8	97
1 (base)	282 (622)	16	9.8	99
		Number of legs:	4	
		Total mass:	2909 kg	
		Total # springs:	144	
		$\log_{10}(T_{zz})$ @ 35Hz:	-4.80	

Table 7: BSC stack design with COIL springs.

The stack is shown in Fig. 10. As mentioned in section 4.2, the leg elements and total stack height are the same as those of the Viton stack.

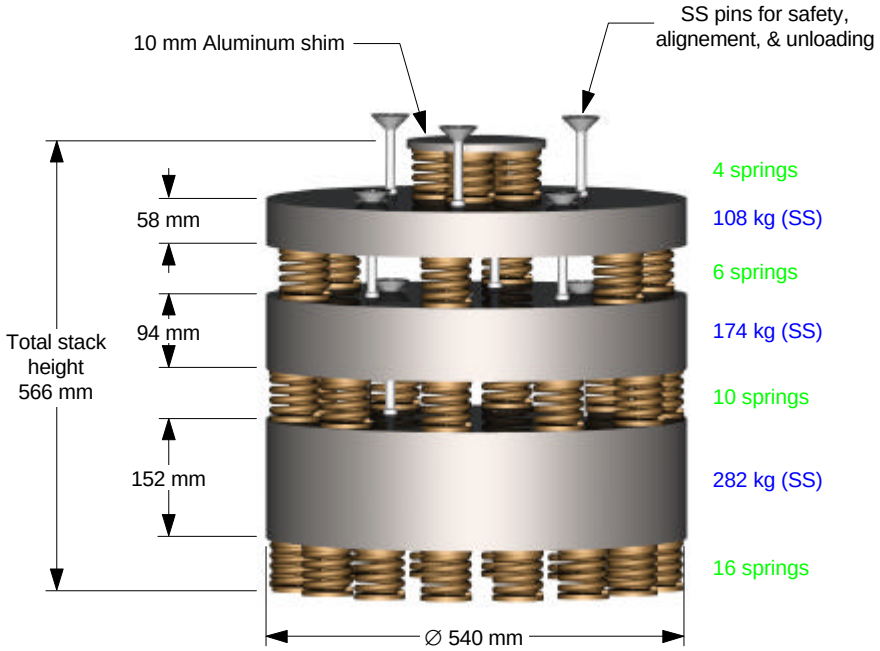

Figure 10: One leg of a COIL spring stack.

5.3 Performance Predictions

Predicted performance of the nominal (perfect) stack is shown in Fig. 11. Note the vast improvement as compared to the Viton stack performance of Fig. 7. The vertical (T_{zz}) requirement is satisfied at all frequencies; however, large resonance peaks at about 15 to 18 Hz cause violations of the horizontal isolation requirement (T_{zz}) in the 12 to 21 Hz range. These peaks are due to a combination of stack resonances (green curve in Fig. 11, left) and the support assembly resonance at 15 Hz.

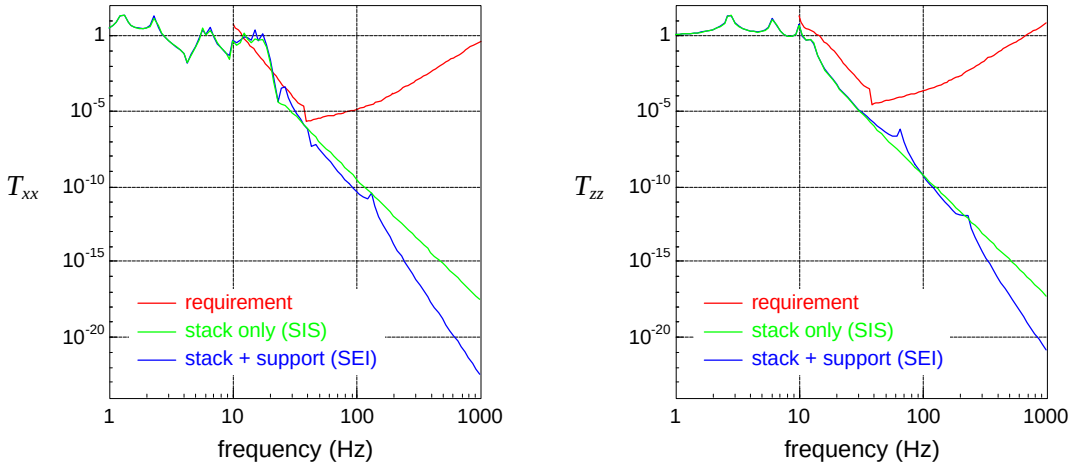

Figure 11: Nominal isolation performance of BSC stack with COIL springs compared to requirements (axial spring properties from analytical predictions, shear properties and number of active turns from experimental results[9]).

Complete Monte Carlo simulation results for imperfect stacks are given in Appendices B.1 and B.2 (also see section 8 for an important note)). As for the Viton stack, the sensitivity to imperfections is small for all terms that do not vanish in a perfect stack.

The predicted spectrum of test mass motion for a stack with flexible support is shown in Fig. 12. Note that the requirement is satisfied at most frequencies, with the exception of the 10 to 22 Hz range where the highest stack resonances produce slight violations (by about 1 order of magnitude). Compared to the performance of a Viton stack however, this shows very dramatic improvement. Note also that this simulation is based on spring properties obtained from analysis (with minor adjustments based on test results) that does not account for the compliance of the Viton seats. These seats will reduce the spring stiffnesses to some extent, leading to further improvements in stack isolation performance.

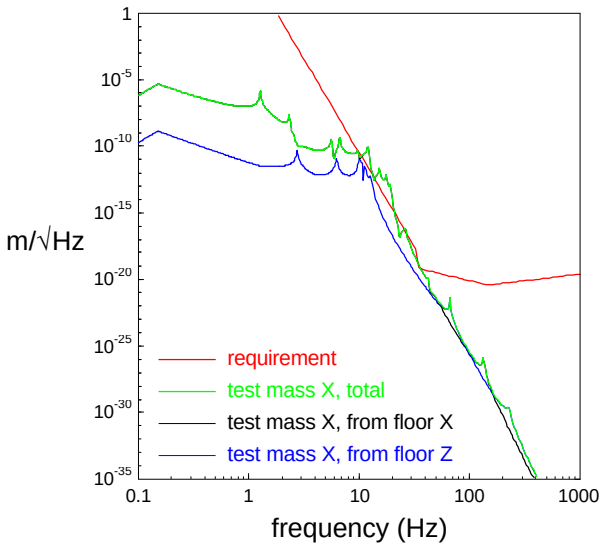

Figure 12: Spectrum of residual test mass X motion for COIL spring stack with flexible support; the green curve shows total residual seismic noise while the black and blue curves show contributions from horizontal and vertical floor noise, respectively.

The values obtained for the lock acquisition and maintenance criteria are listed in Table 8 and compared to requirements. The lock acquisition figure of merit is substantially higher than for the Viton stack because of the higher Q of the first few resonances of the stack. Sufficient experimental data is ***not*** available at this point to determine those Q's with any reasonable accuracy. The ***most pessimistic*** estimates would lead to a first stack resonance at 1.28 Hz, with a Q of 85. This value of Q results from the very sharp decrease in damping at low frequency predicted by analysis of the spring[6] (but not yet confirmed by measurements) and does not account for the additional damping expected from the Viton seats. In fact, experimental evidence acquired so far[9] would lead to estimates of the Q's in the 40 to 60 range. We need to stress however that those estimates should not be taken for granted before measured values are available at low frequency (1 to 2 Hz range).

	value	requirement
Lock Acquisition	2.50 μm/sec	~ 1 μm/sec
Lock Maintenance	2.45 μm	< 2.7 μm

Table 8: BSC stack with coil springs. Lock acquisition and maintenance requirements (no difference between stack only and support included).

6. Leaf Spring Stack

6.1 Properties of Leaf Spring

These springs (Fig. 13) are described in detail in [6]. Their expected static axial load capacity is 556 N (125 lbs).

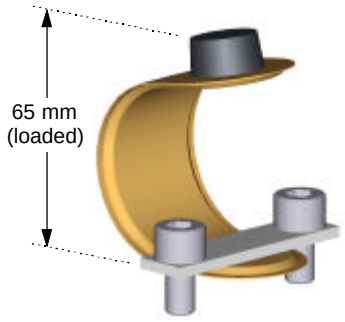

Figure 13: leaf spring geometry (shown unloaded).

Dynamic properties (stiffness and damping vs frequency) were obtained from FEM analysis as described in [6]. The detailed design of the interfaces with the leg elements is not completely defined at this time; it is expected however, that the height under load of those springs will be the same as that of the coil springs, providing again a direct back and forth compatibility with the other two stacks.

6.2 Stack Design

The stack design procedure[5] with a maximum load per spring equal to 556 N (125 lbs) leads to the stack design of Table 9. Note again that the total weight of this stack is identical to that of the baseline Viton stack of Table 5.

i (stage #)	M_i, kg (lb) (per leg)	# *springs / leg*	f_i (Hz)	P_i/P_{max} (%)
4 (top)	163 (359)	3	6.7	96
3	108 (239)	5	10.2	96
2	174 (383)	8	10.2	98
1 (base)	282 (622)	13	10.2	99
		Number of legs:	4	
		Total mass:	2909 kg	
		Total # springs:	116	
		$\log_{10}(T_{zz})$ @ 35Hz:	-4.68	

Table 9: BSC stack design with LEAF springs.

Again, this stack uses the same leg elements as both the Viton spring stack and the Coil spring stack and occupies the same vertical space (Fig. 14).

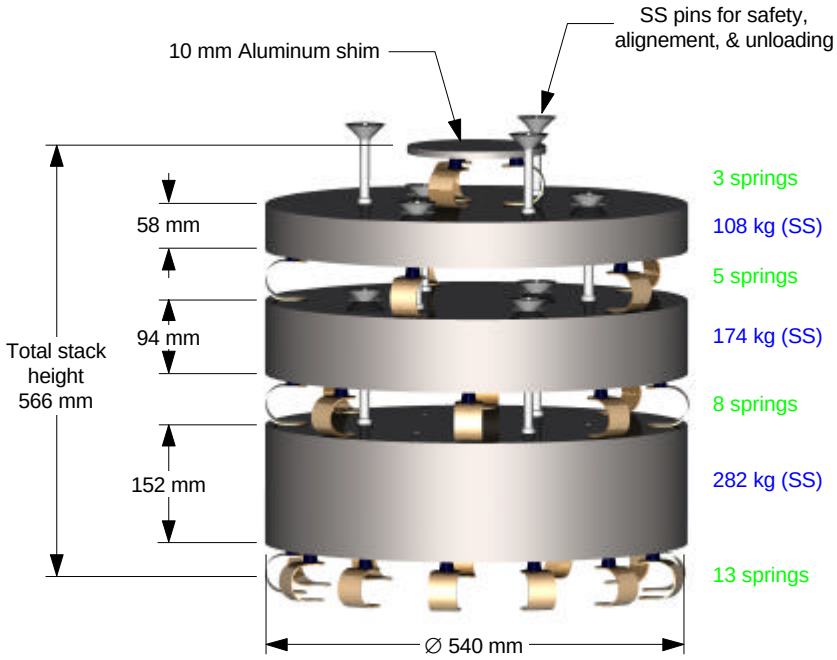

Figure 14: One leg of a LEAF spring stack.

6.3 Performance Predictions

Predicted performance of the nominal (perfect) stack is shown in Fig. 15. As with the coil spring stack, performance is vastly improved as compared to the Viton stack performance of Fig. 7. Note that this prediction is based on pre-test spring data that does not include the Viton interface pad at the top of the leaf spring (see Fig. 13); this pad is expected to reduce the spring stiffness somewhat, leading to marked improvements in performance.

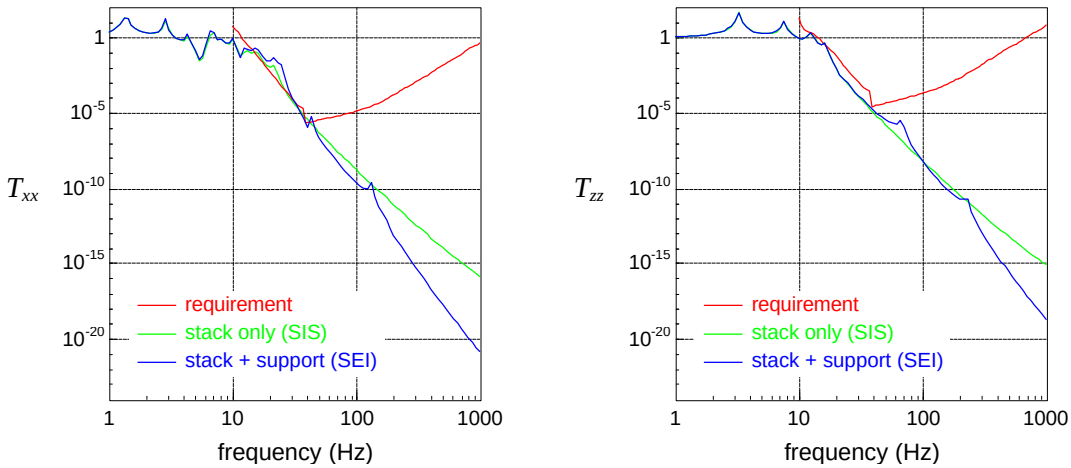

Figure 15: Nominal isolation performance of BSC stack with LEAF springs compared to requirements (spring properties from pre-test analytical predictions)

Complete Monte Carlo simulation results for imperfect stacks are given in Appendices C1 and C2 (also see section 8 for an important note). Again, sensitivity to imperfections is small for all terms that do not vanish in a perfect stack. Predicted test mass motion in the *X* direction for a stack with flexible support are shown in Fig. 16. Note the slight violation of the requirements in the 10 to 40 Hz range. Also, the figure gives the contributions to test mass motion from floor X noise alone (black curve) and floor Z noise alone (blue curve); the direct transmission from floor X noise is by far the dominant contribution at frequencies below about 35 Hz.

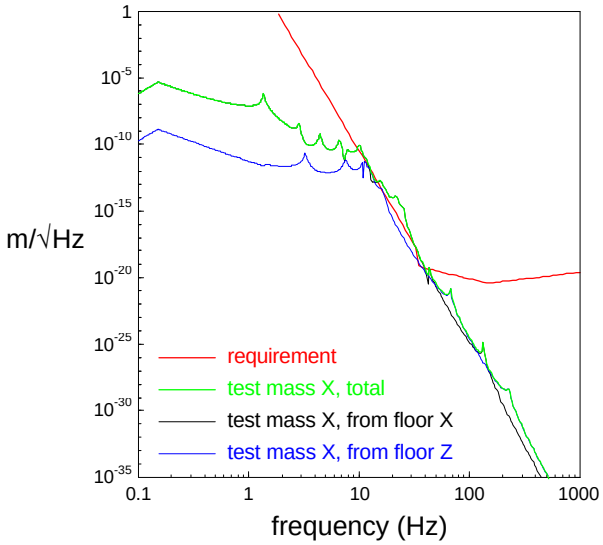

Figure 16: Spectrum of residual test mass X motion for LEAF spring stack with flexible support; the green curve shows total residual seismic noise while the black and blue curves show contributions from horizontal and vertical floor noise, respectively.

The values obtained for the lock acquisition and maintenance criteria are listed in Table 10 and compared to requirements.

	value	requirement
Lock Acquisition	1.88 μm/sec	~ 1 μm/sec
Lock Maintenance	2.27 μm	< 2.7 μm

Table 10: BSC stack design with LEAF springs. Lock acquisition and maintenance requirements (no difference between stack only and support included).

7. References

1. B. Weinstein, *BSC Support Assembly - Analytical Design*, HYTEC Inc., Los Alamos, NM, document HYTEC-TN-LIGO-06a (revision *a*), January 1997.
2. E. Ponslet, *Isolation Stacks Preliminary Design Methodology*, HYTEC Inc., Los Alamos, NM, document HYTEC-TN-LIGO-02, February 21, 1996.
3. E. Ponslet and B. Weinstein, *BSC Downtube Structure - Mechanical Design and analysis*, HYTEC Inc., Los Alamos, NM, document HYTEC-TN-LIGO-05a (revision *a*), January 1997.
4. F. Raab and N. Solomonson, *Seismic Isolation Design Requirements Document* (draft and early corrections), LIGO draft document LIGO-T960065-02-D, California Institute of Technology and Massachusetts Institute of Technology, April 15, 1996.
5. E. Ponslet, *BSC Stack Design Trend Study*, HYTEC Inc., Los Alamos, NM, document HYTEC-TN-LIGO-03, March 1st, 1996.
6. E. Ponslet, *Design of Vacuum Compatible Damped Metal Springs for Passive Isolation of The LIGO Detectors*, HYTEC Inc., Los Alamos, NM, document HYTEC-TN-LIGO-04a (revision *a*), January 1997.
7. F. Raab, California Institute of Technology, private communication, August 1996.
8. S. Kawamura, *Response of Pendulum to Motion of Suspension Point*, LIGO document LIGO-T960040-00-D, California Institute of Technology and Massachusetts Institute of Technology, March 11, 1996.
9. E. Ponslet, *LIGO Coil Springs - Test Report*, HYTEC Inc., Los Alamos, NM, document HYTEC-TN-LIGO-14, February 1997.
10. S. Kawamura, *Response of Suspension System to Pitch Motion of Suspension Point*, LIGO document LIGO-T960158-00-D, California Institute of Technology and Massachusetts Institute of Technology, September 26, 1996.

8. Note About Monte-Carlo Simulation Results in Appendices

Because of extensive CPU time required to run Monte-Carlo simulations, all results presented in the following appendices were obtained for an earlier version of the stacks and support models; these results are not directly comparable to those presented in the rest of this note. However, these appendices do illustrate the fact that all significant transmissibility terms are relatively insensitive to imperfections in the actual stacks and support systems. Because of this, further investigations of imperfection effects are unnecessary.

Each figure in the appendices shows 3 curves: the black curve is the transmissibility of the nominal (perfect) stack while the two green curves represent upper and lower limits of the transmissibilities of imperfect stacks. In addition, when appropriate, the corresponding requirement is shown in red. Note that, for transmissibilities that do not vanish for a perfect stack, the nominal performance is inside the range defined by the green curves and that in most cases that range is extremely narrow. For terms that vanish in a perfect stack, the black curve really shows numerical noise and the green curves define a

larger range. That range does not include the nominal performance because any small imperfection makes those terms jump from zero to a non-zero value.

9. Appendix A.1: Transmissibilities of Viton Spring SIS (stack only)

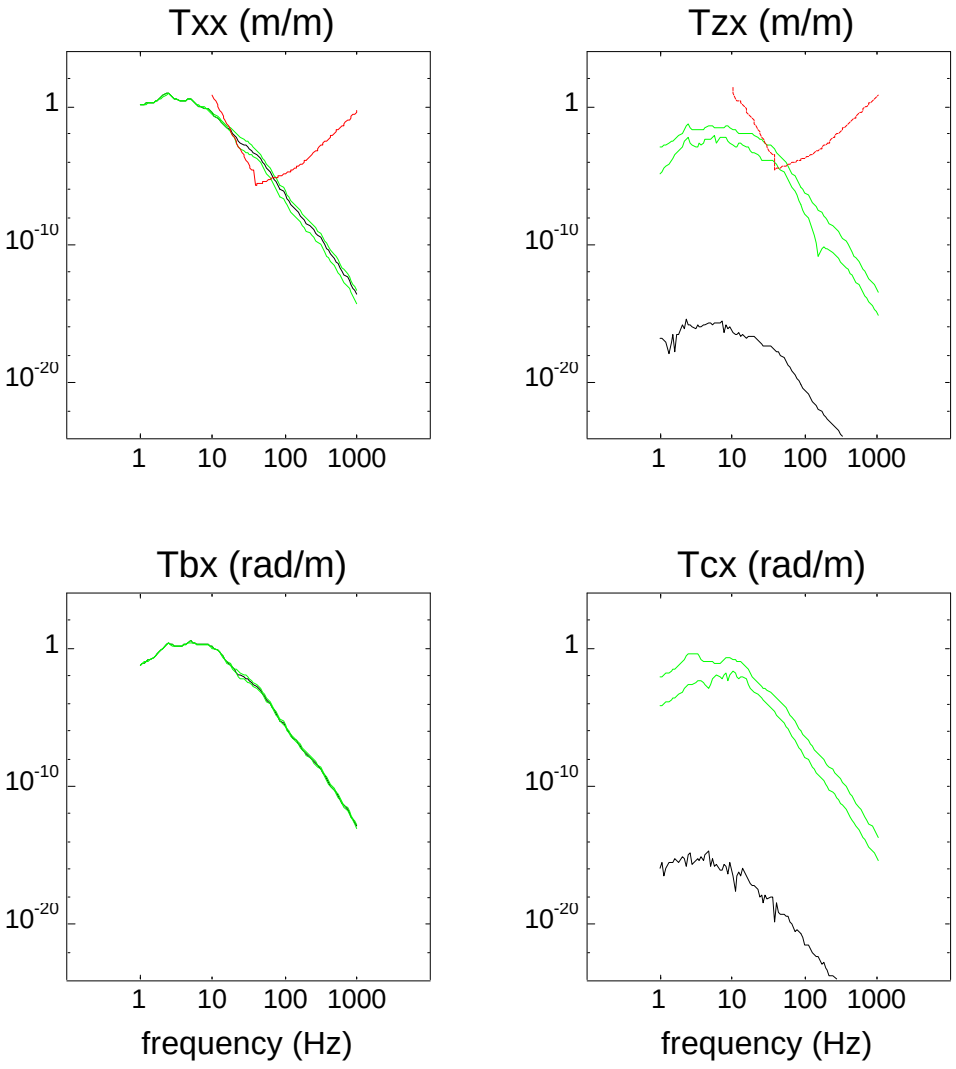

Figure 17: SIS with Viton Springs (stack only); transmissibilities from floor motion in horizontal (*X*) direction to pendulum suspension point motion in horizontal (*X*), vertical (*Z*), pitch (*b*), and yaw (*c*) directions.

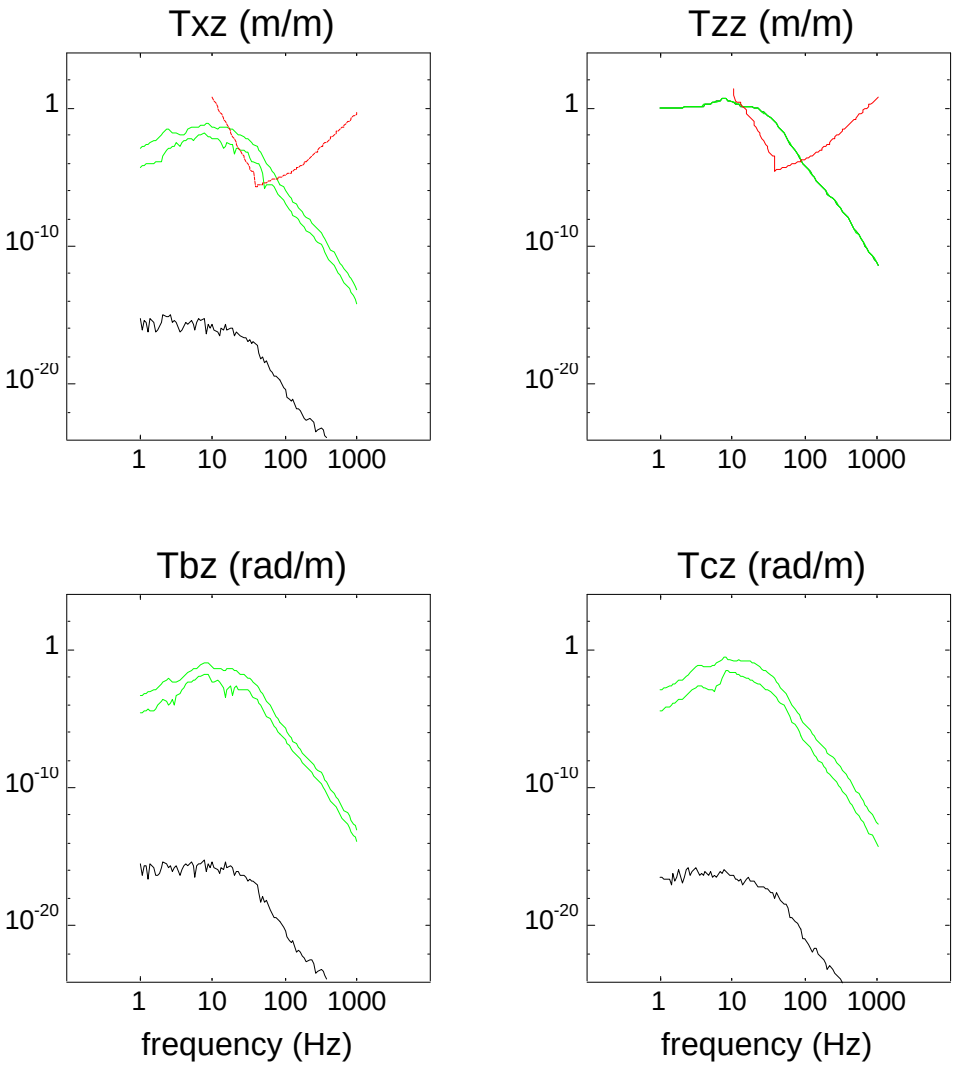

Figure 18: SIS with Viton Springs (stack only); transmissibilities from floor motion in vertical (*Z*) direction to pendulum suspension point motion in horizontal (*X*), vertical (*Z*), pitch (*b*), and yaw (*c*) directions.

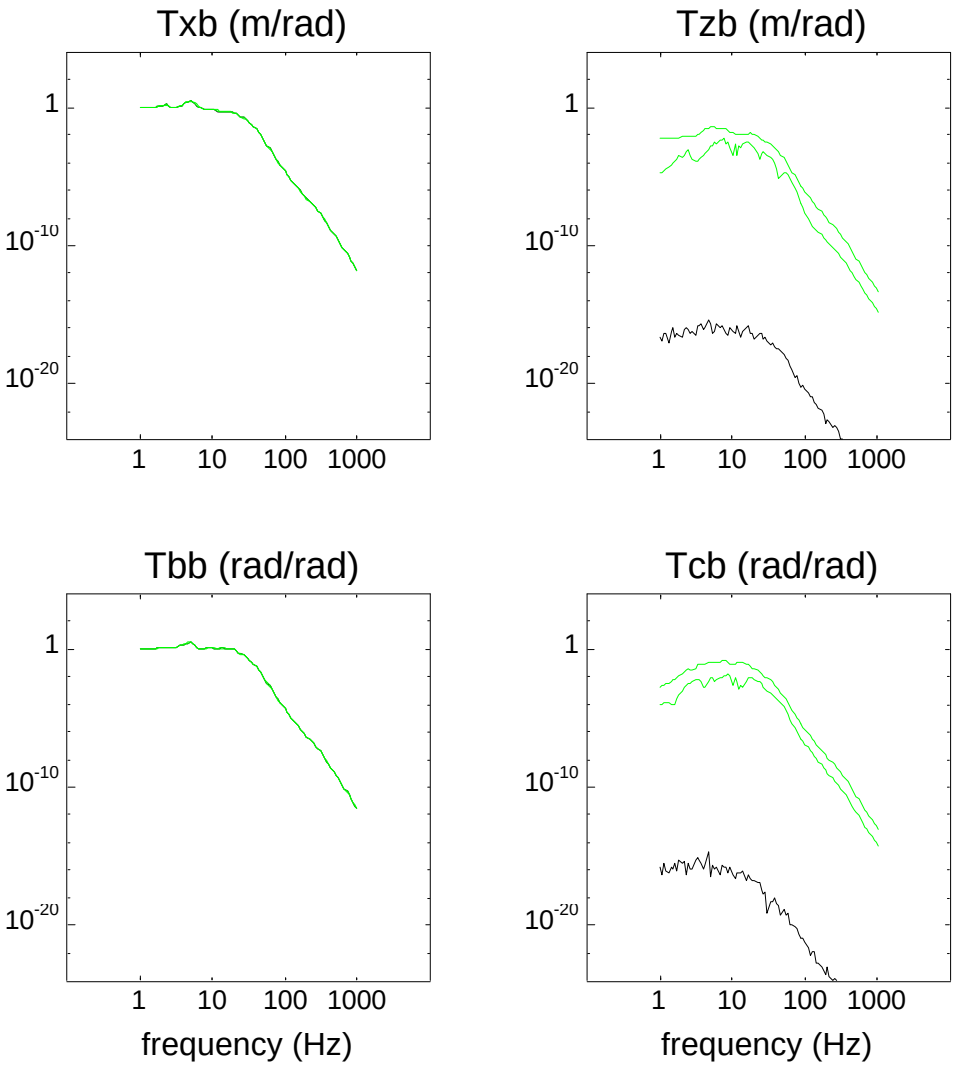

Figure 19: SIS with Viton Springs (stack only); transmissibilities from floor motion in pitch (*b*) direction to pendulum suspension point motion in horizontal (*X*), vertical (*Z*), pitch (*b*), and yaw (*c*) directions.

10. Appendix A2: Transmissibilities of Viton spring SEI (support included)

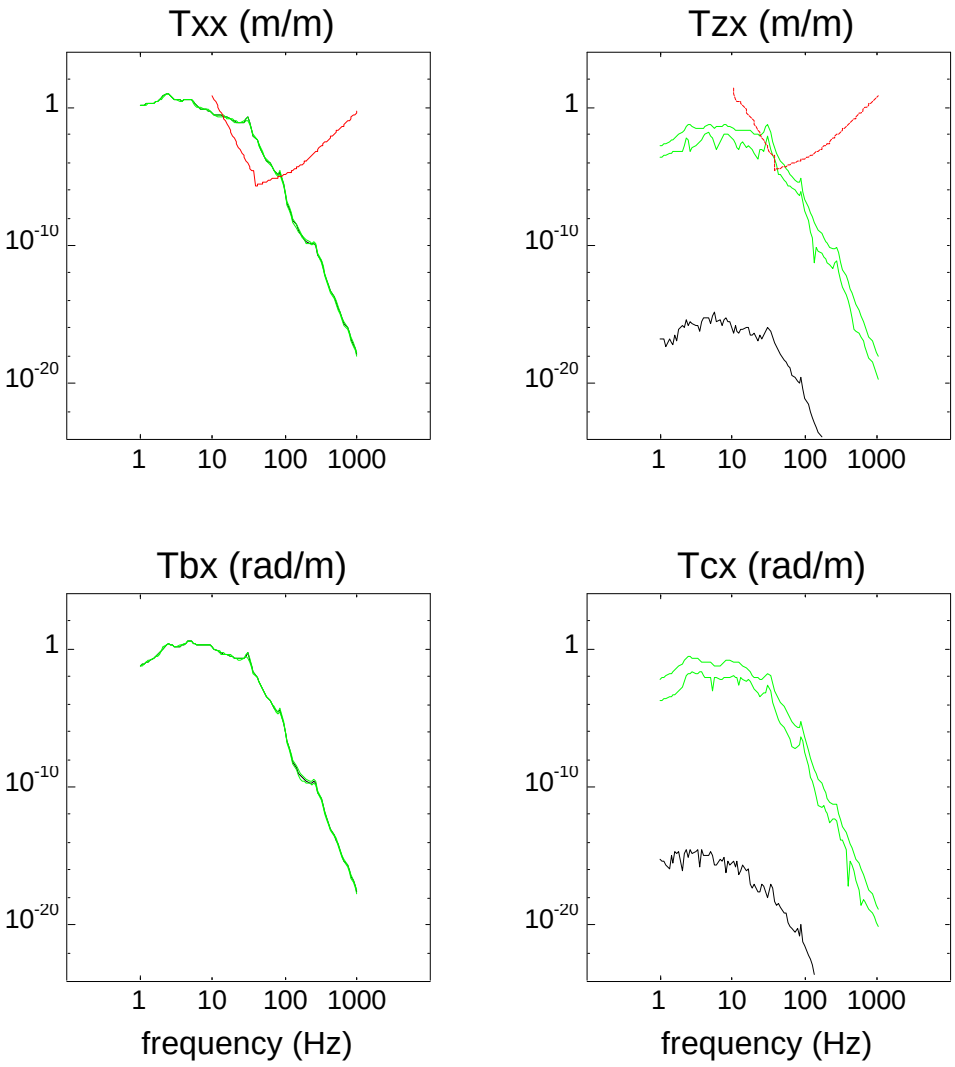

Figure 20: SEI with Viton Springs (support included); transmissibilities from floor motion in horizontal (*X*) direction to pendulum suspension point motion in horizontal (*X*), vertical (*Z*), pitch (*b*), and yaw (*c*) directions.

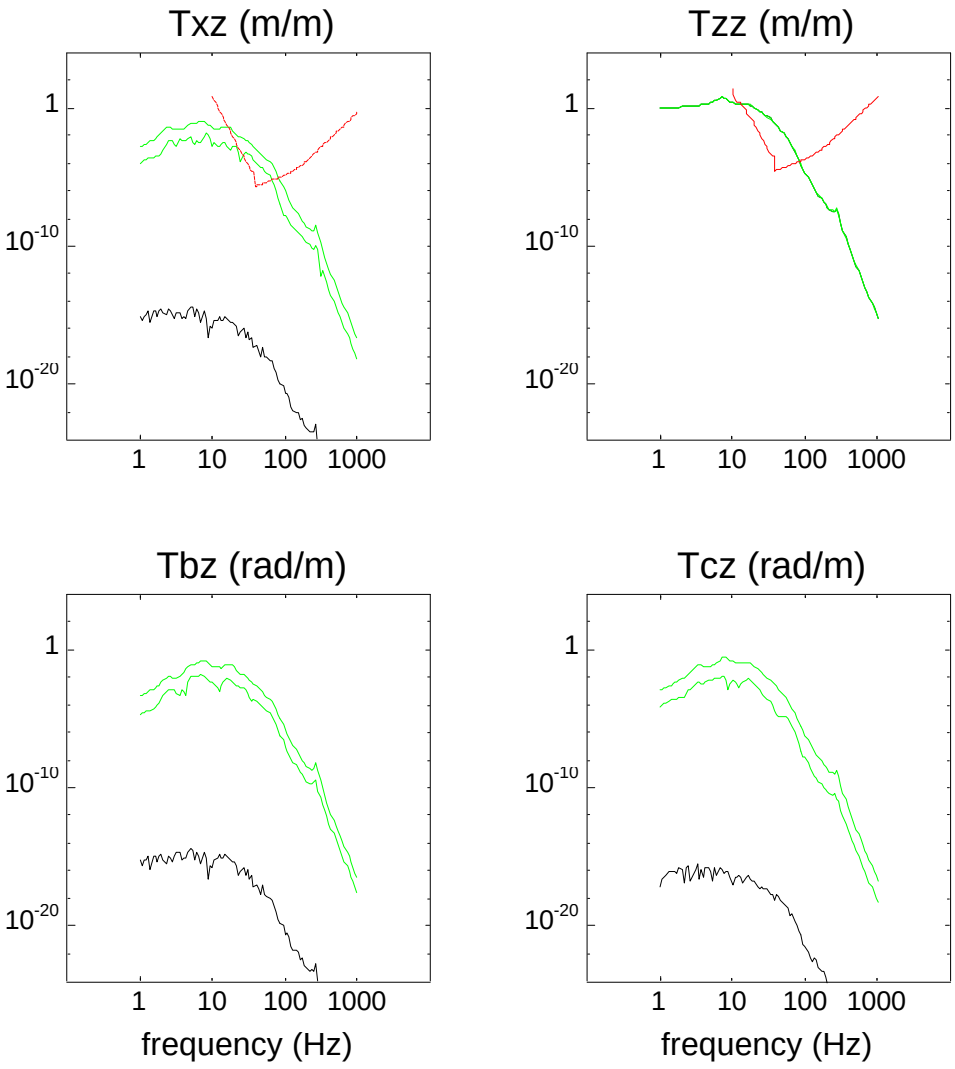

Figure 21: SEI with Viton Springs (support included); transmissibilities from floor motion in vertical (*Z*) direction to pendulum suspension point motion in horizontal (*X*), vertical (*Z*), pitch (*b*), and yaw (*c*) directions.

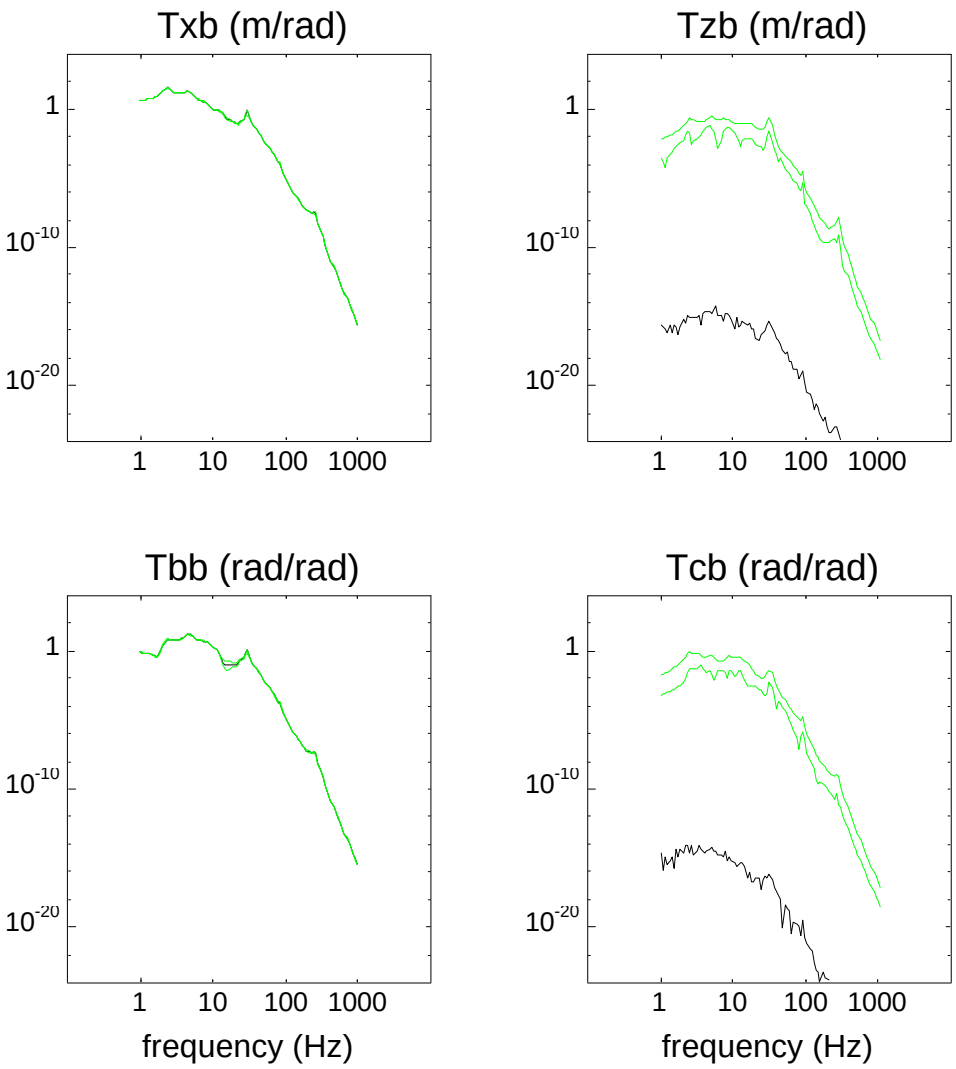

Figure 22: SEI with Viton Springs (support included); transmissibilities from floor motion in pitch (*b*) direction to pendulum suspension point motion in horizontal (*X*), vertical (*Z*), pitch (*b*), and yaw (*c*) directions.

11. Appendix B.1: Transmissibilities of Coil Spring SIS (stack only)

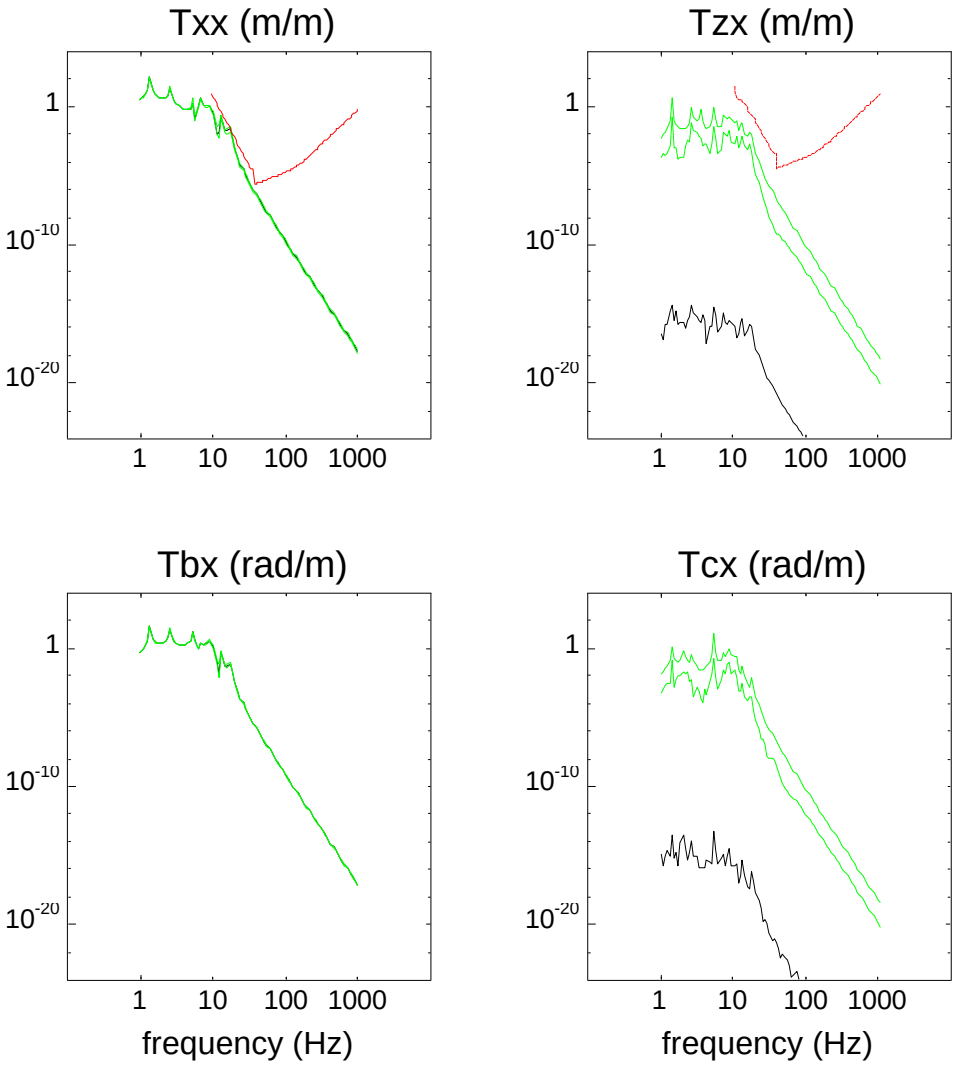

Figure 23: SIS with Coil Springs (stack only); transmissibilities from floor motion in horizontal (*X*) direction to pendulum suspension point motion in horizontal (*X*), vertical (*Z*), pitch (*b*), and yaw (*c*) directions.

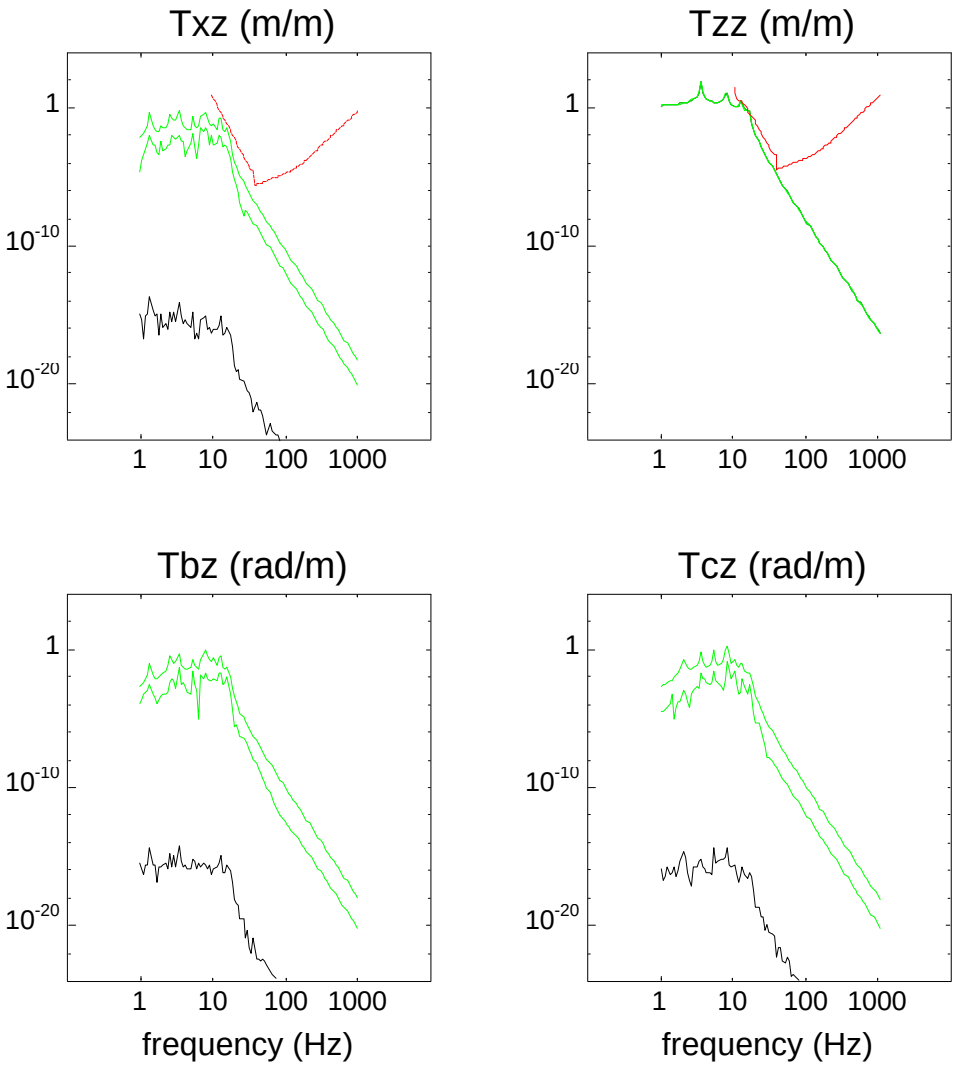

Figure 24: SIS with Coil Springs (stack only); transmissibilities from floor motion in vertical (*Z*) direction to pendulum suspension point motion in horizontal (*X*), vertical (*Z*), pitch (*b*), and yaw (*c*) directions.

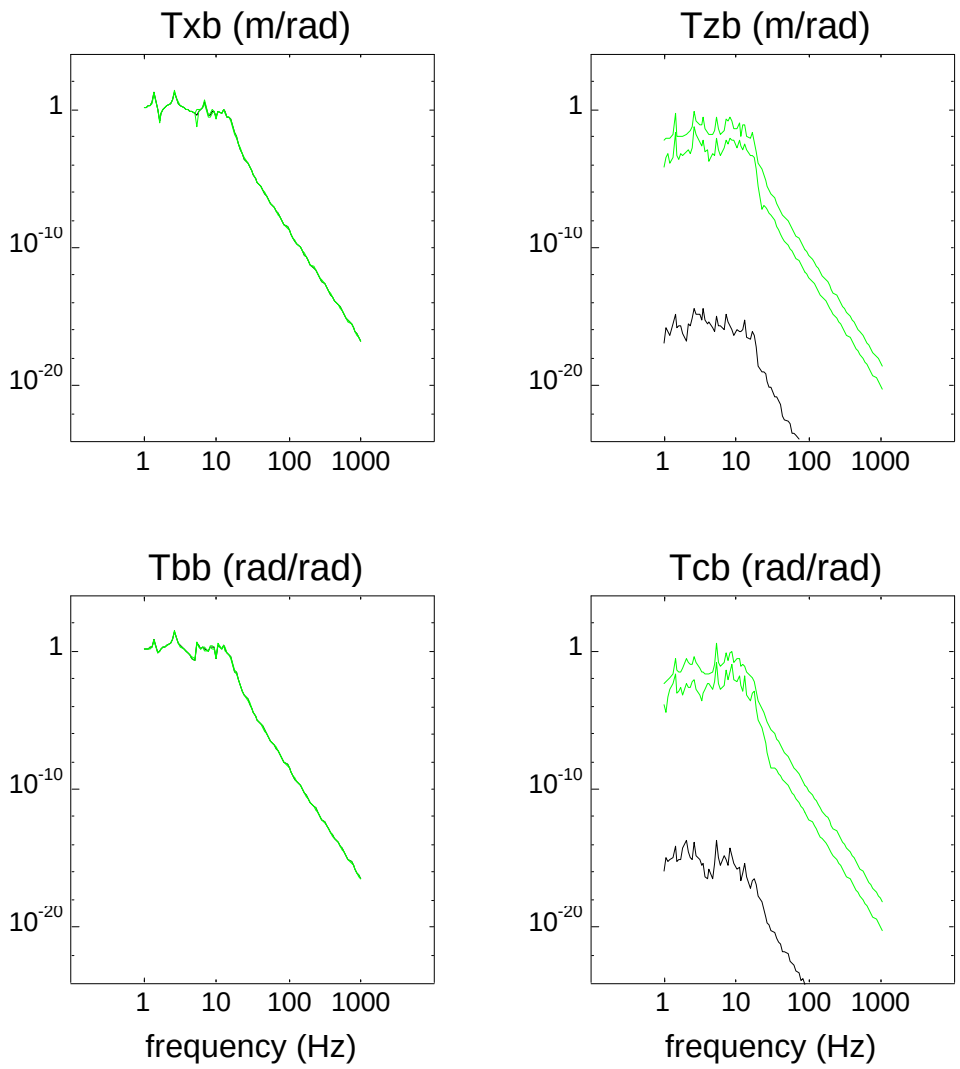

Figure 25: SIS with Coil Springs (stack only); transmissibilities from floor motion in pitch (*b*) direction to pendulum suspension point motion in horizontal (*X*), vertical (*Z*), pitch (*b*), and yaw (*c*) directions.

12. Appendix B.2: Transmissibilities of Coil Spring SEI (support included)

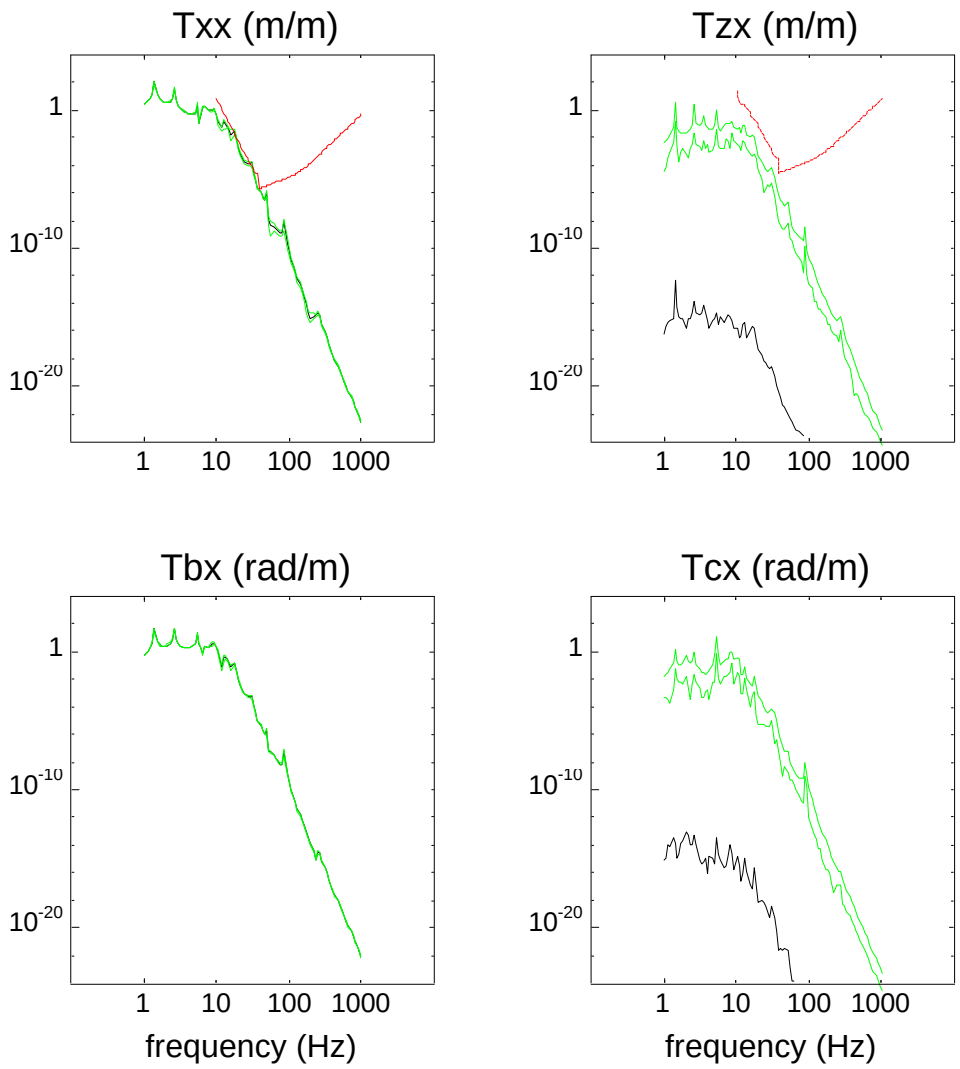

Figure 26: SEI with Coil Springs (support included); transmissibilities from floor motion in horizontal (*X*) direction to pendulum suspension point motion in horizontal (*X*), vertical (*Z*), pitch (*b*), and yaw (*c*) directions.

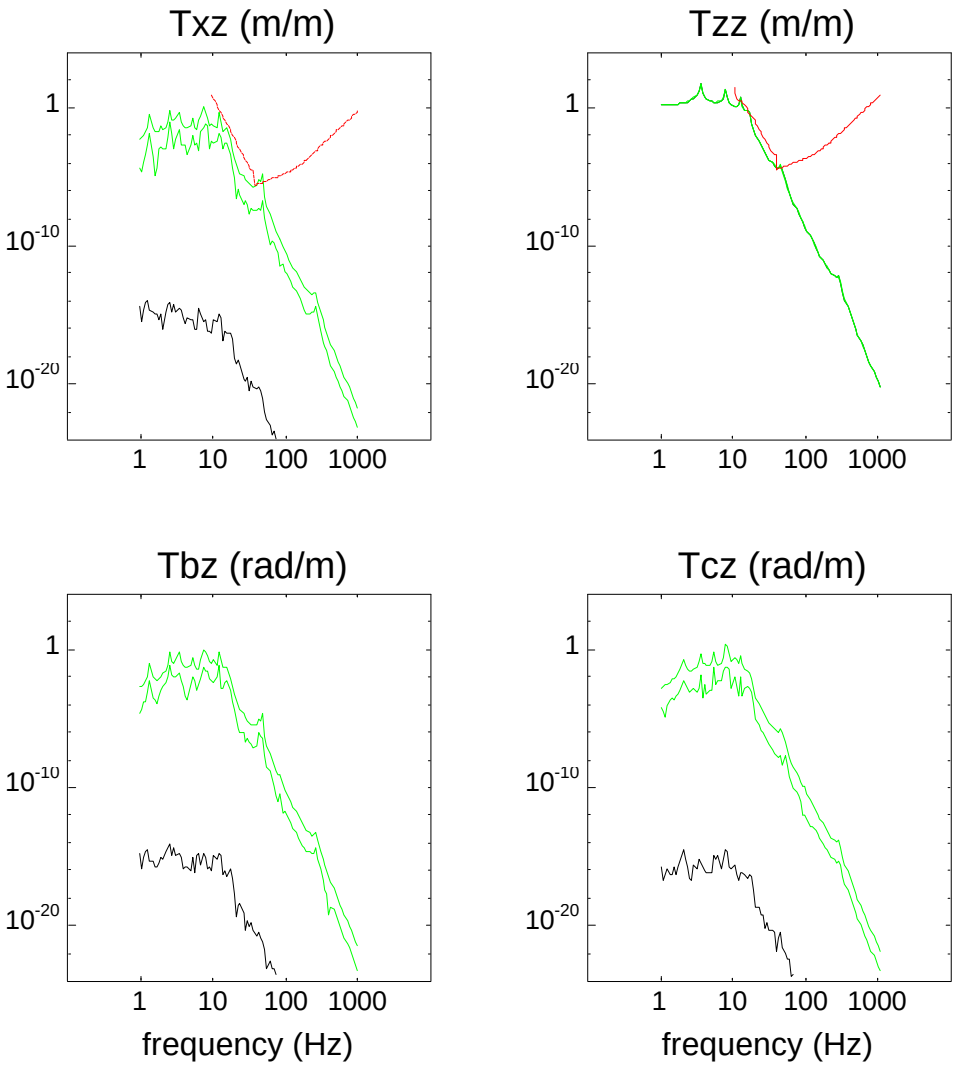

Figure 27: SEI with Coil Springs (support included); transmissibilities from floor motion in vertical (*Z*) direction to pendulum suspension point motion in horizontal (*X*), vertical (*Z*), pitch (*b*), and yaw (*c*) directions.

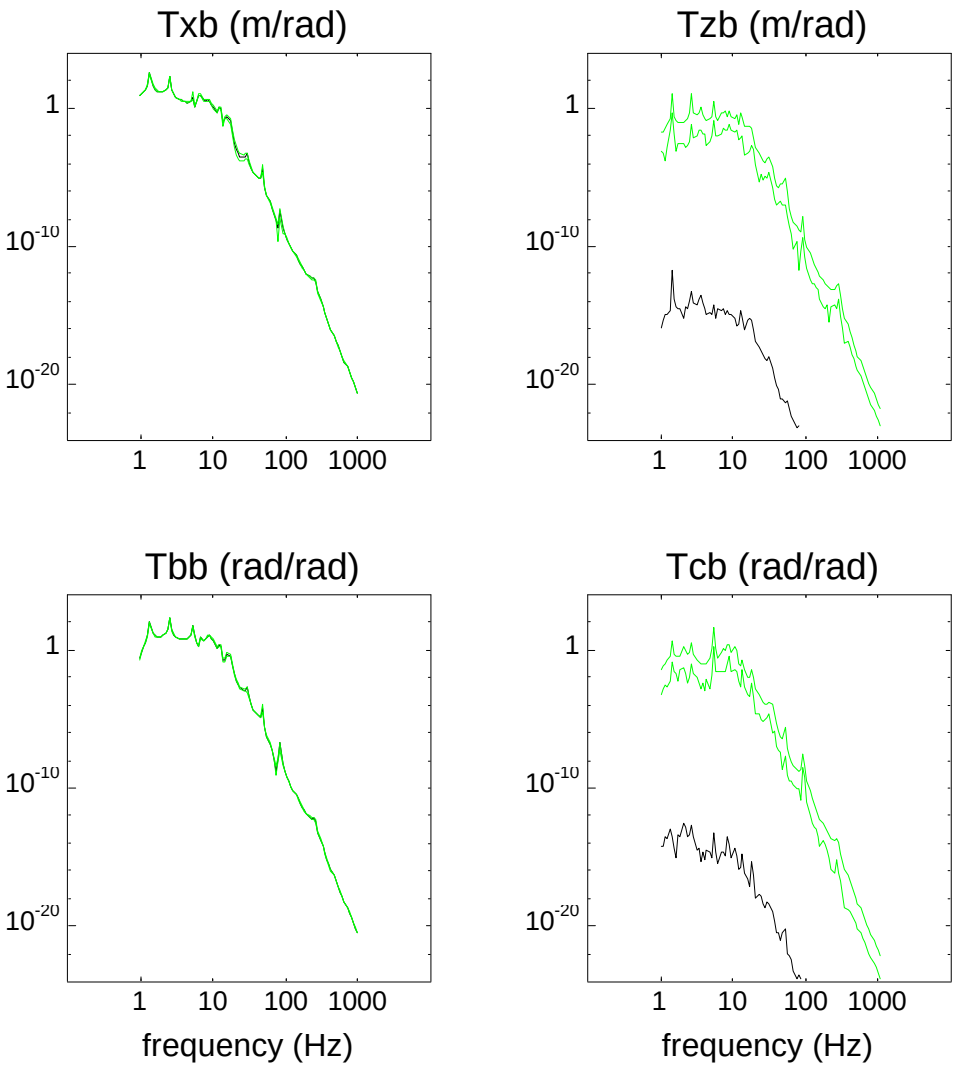

Figure 28: SEI with Coil Springs (support included); transmissibilities from floor motion in pitch (*b*) direction to pendulum suspension point motion in horizontal (*X*), vertical (*Z*), pitch (*b*), and yaw (*c*) directions.

13. Appendix C.1: Transmissibilities of Leaf Spring SIS (stack only)

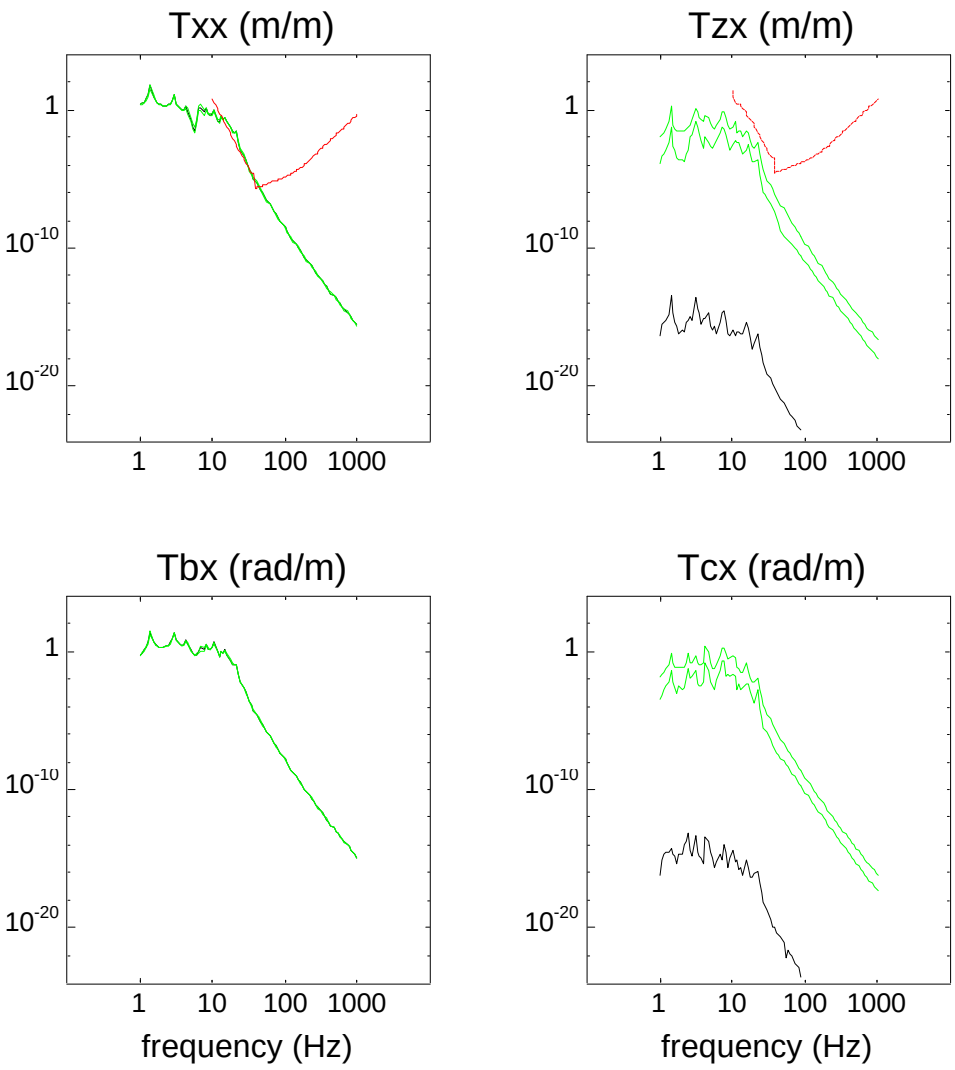

Figure 29: SIS with Leaf Springs (stack only); transmissibilities from floor motion in horizontal (*X*) direction to pendulum suspension point motion in horizontal (*X*), vertical (*Z*), pitch (*b*), and yaw (*c*) directions.

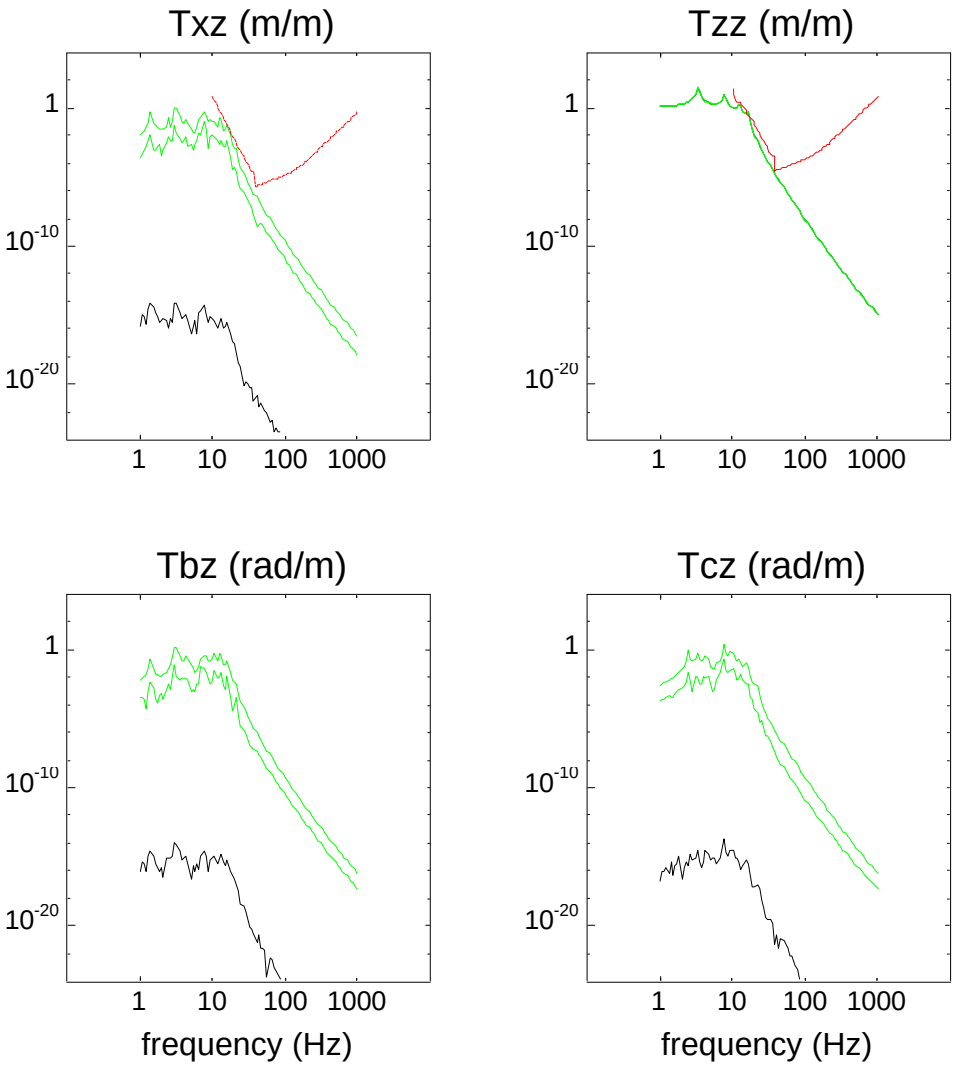

Figure 30: SIS with Leaf Springs (stack only); transmissibilities from floor motion in vertical (*Z*) direction to pendulum suspension point motion in horizontal (*X*), vertical (*Z*), pitch (*b*), and yaw (*c*) directions.

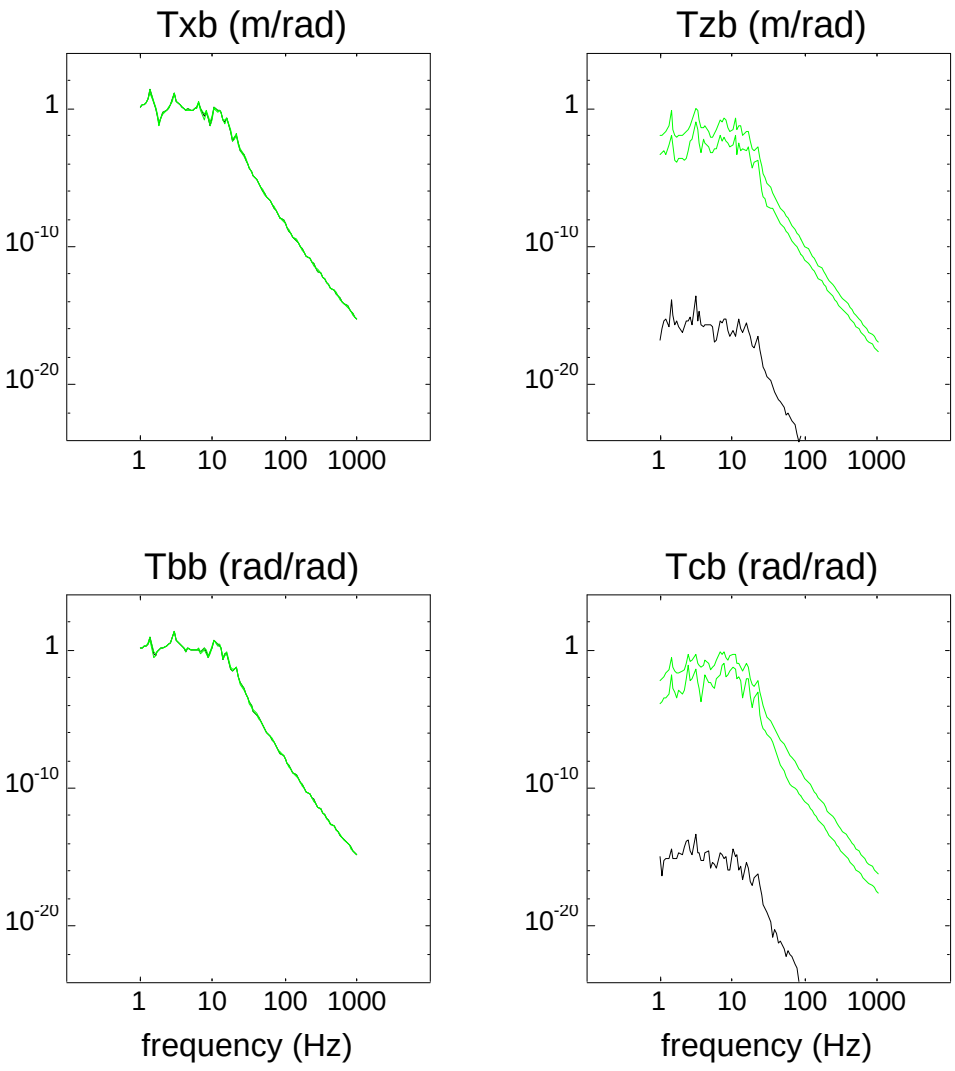

Figure 31: SIS with Leaf Springs (stack only); transmissibilities from floor motion in pitch (*b*) direction to pendulum suspension point motion in horizontal (*X*), vertical (*Z*), pitch (*b*), and yaw (*c*) directions.

14. Appendix C.2: Transmissibilities of Leaf Spring SEI (support included)

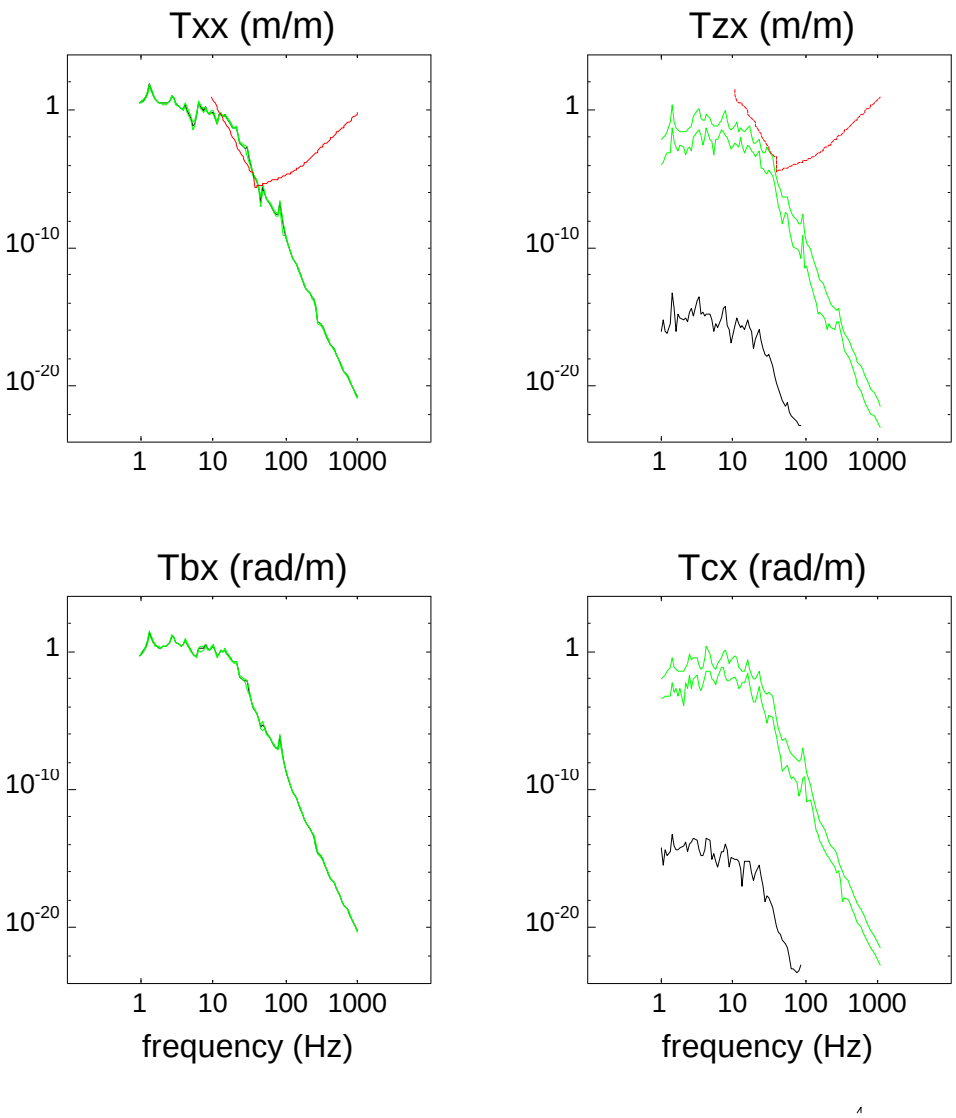

Figure 32: SEI with Leaf Springs (support included); transmissibilities from floor motion in horizontal (*X*) direction to pendulum suspension point motion in horizontal (*X*), vertical (*Z*), pitch (*b*), and yaw (*c*) directions.

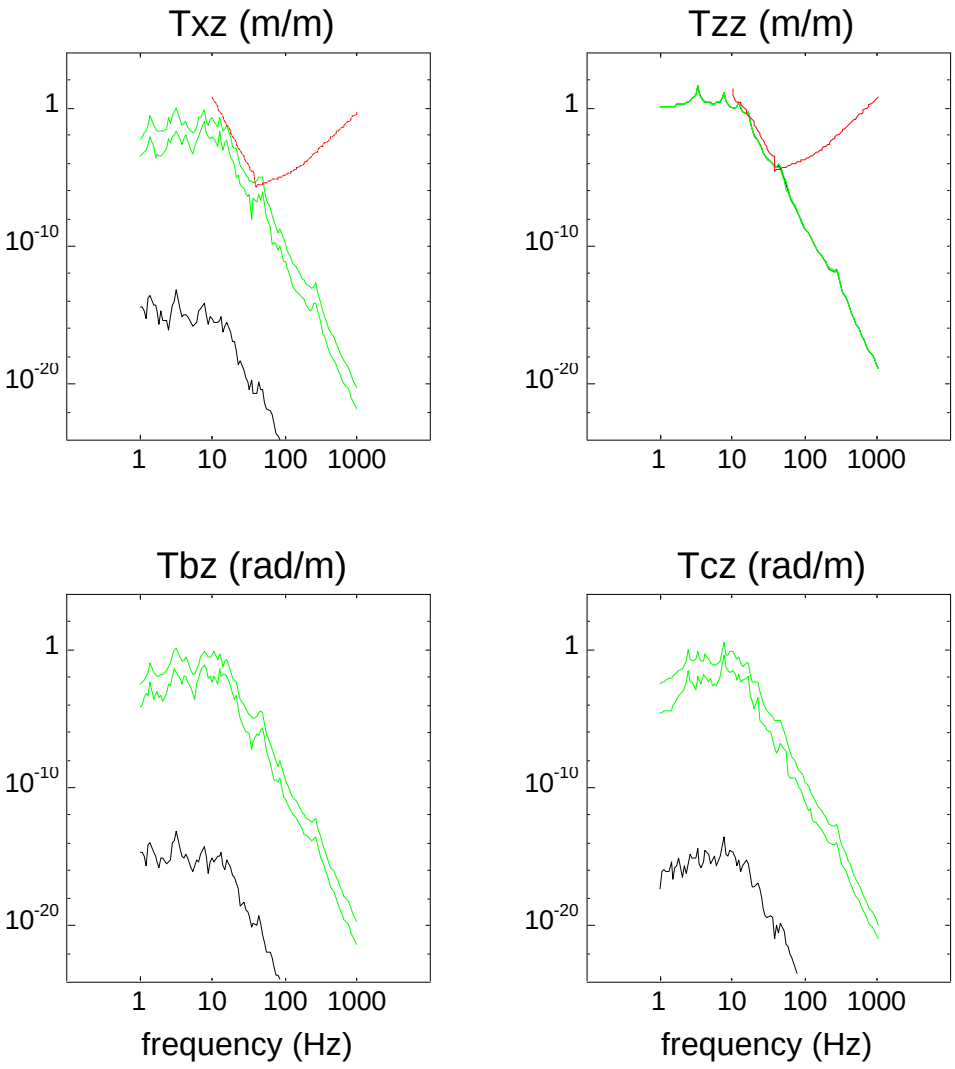

Figure 33: SEI with Leaf Springs (support included); transmissibilities from floor motion in vertical (*Z*) direction to pendulum suspension point motion in horizontal (*X*), vertical (*Z*), pitch (*b*), and yaw (*c*) directions.

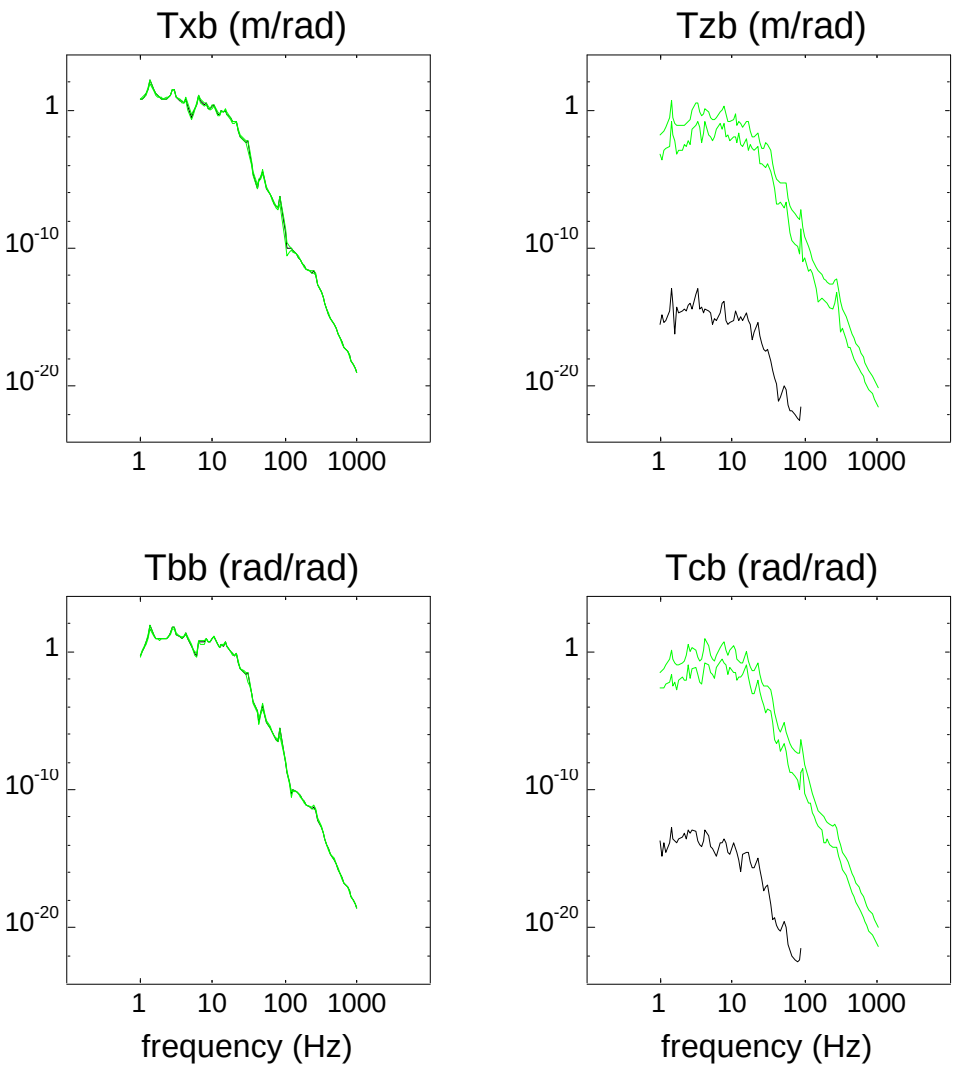

Figure 34: SEI with Leaf Springs (support included); transmissibilities from floor motion in pitch (*b*) direction to pendulum suspension point motion in horizontal (*X*), vertical (*Z*), pitch (*b*), and yaw (*c*) directions.

Note 1, Linda Turner, 09/03/99 11:32:31 AM
LIGO-T960215-A-D